Global and Planetary Change 257 (2026) 105208

Contents lists available at ScienceDirect

Global and Planetary Change

journal homepage: www.elsevier.com/locate/gloplacha

Research Article

Algal reorganization in post-crisis Early Triassic oceans revealed by biomarker evidence☆

Yizhou Huang [a,b,*], B. David A. Naafs [a], Li Tian [b], Stephen E. Grasby [c,d], David P.G. Bond [e], Paul B. Wignall [f], Michael J. Benton [g], Richard D. Pancost [a]

[a] Organic Geochemistry Unit, School of Chemistry, School of Earth Sciences, Cabot Institute of the Environment, University of Bristol, Bristol BS8 1TS, UK
[b] State Key Laboratory of Geomicrobiology and Environmental Changes, China University of Geosciences, Wuhan 430074, China
[c] Geological Survey of Canada, 3303 33 Street NW, Calgary, Alberta T2L 2A7, Canada
[d] Department of Geoscience, University of Calgary, 2500 University Drive NW, Calgary, Alberta T2N 1N4, Canada
[e] School of Environmental and Life Sciences, University of Hull, Hull HU6 7RX, UK
[f] School of Earth and Environment, University of Leeds, Leeds LS2 9JT, UK
[g] Palaeobiology Research Group, School of Earth Sciences, University of Bristol, Bristol BS8 1RJ, UK

ARTICLE INFO

Editor: Dr. Maoyan Zhu

Dataset link: Biomarker data for Algal reorganization in post-crisis Early Triassic oceans revealed by biomarker evidence (Original data)

Keywords:
Eukaryotic algae
Regular sterane
Primary production
Marine ecosystem
Early Triassic

ABSTRACT

The end-Permian mass extinction (EPME) fundamentally reshaped marine ecosystems. However, the long-term response of eukaryotic algae, a key foundation for marine primary production, is poorly understood. To address this limited knowledge, we determine the long-term change in algal communities using molecular fossil steranes. We use samples that span the uppermost Permian to the Lower Triassic from sections that were located in Boreal Sea (Sverdrup Basin, Arctic Canada) as well as the tropical Tethys (Xiakou, South China), and complement these new data with published datasets. Sterane to hopane ratios, reflecting the relative contribution of eukaryotic algal to bacterial sources, vary in absolute values between sites but show no significant decrease in the earliest Griesbachian compared to the pre-crisis Permian. However, Early Triassic ratios changed dramatically. In the Sverdrup Basin, they were stable during the Griesbachian and, following an interval where both hopane and sterane concentrations diminished, became much higher in the late Spathian. This confirms suggestions that there was a major decline in algal productivity after the EPME that may have delayed recovery. Sterane C_{28}/C_{29} ratios, which monitor algal composition, increase at the EPME level in Meishan and are generally higher in the rest of the Early Triassic in the Sverdrup Basin and Chaohu. The increase shows that algae that preferentially produce C_{28} over C_{29} sterols were thriving, possibly including those predominant in modern oceans. It further implies a reorganized marine algal community–apparently in the tropics and in the post-crisis interval in the Boreal realm. Our findings suggest that instead of a simple collapse and recovery, the Early Triassic saw a complicated reorganisation for algae.

1. Introduction

The end-Permian Mass Extinction (EPME) severely impacted marine and terrestrial organisms (Algeo et al., 2011; Benton and Newell, 2014; Bond and Grasby, 2017; Chen and Benton, 2012; Dal Corso et al., 2020, 2022; Shen et al., 2011; Wignall, 2007; Wignall et al., 2020a), including the primary producers that are the foundation of ecosystems (Falkowski et al., 2004; Payne and van de Schootbrugge, 2007). Marine ecosystems collapsed, and diverse communities were replaced by much-simplified ecological structures (Chen and Benton, 2012; Feng et al., 2022; Galfetti et al., 2008; Knoll et al., 2007a).

The Triassic biotic recovery lasted for 1–2 Myr for benthic communities (Song et al., 2011; Stanley, 2009) but up to 5–10 Myr for more complex ecosystems (Chen and Benton, 2012). This biotic recovery is unusually prolonged in comparison to other mass extinction recoveries (Chen and Benton, 2012; Sahney and Benton, 2008). The mechanisms driving this unusually prolonged recovery are debated, but various climatic and environmental factors and/or interactions within the

☆ This article is part of a Special issue entitled: 'Oceanic Anoxic Event' published in Global and Planetary Change.

* Corresponding author. Present address: State Key Laboratory of Geomicrobiology and Environmental Changes, China University of Geosciences, Wuhan 430074, China. This study was conducted primarily at Organic Geochemistry Unit, University of Bristol.
E-mail address: yizhouhuang@cug.edu.cn (Y. Huang).

https://doi.org/10.1016/j.gloplacha.2025.105208
Received 20 April 2025; Received in revised form 24 November 2025; Accepted 28 November 2025
Available online 29 November 2025
0921-8181/© 2026 The Authors. Published by Elsevier B.V. This is an open access article under the CC BY license (http://creativecommons.org/licenses/by/4.0/).

ecosystem are commonly invoked, including recurrent marine anoxia/euxinia (e.g., Grasby et al., 2013; Grice, 2005; Lau et al., 2016; Wignall and Twitchett, 1996, 2002), nutrient limitation (Grasby et al., 2016; Knies et al., 2013, 2022), an ammonium ocean (Sun et al., 2019), a protracted lethal hothouse (Joachimski et al., 2020; Sun et al., 2012), and ocean acidification (Beauchamp and Grasby, 2012; Clarkson et al., 2015; Fraiser and Bottjer, 2007; Payne et al., 2010; Song et al., 2021).

These proposed mechanisms invoke divergent views about post-EPME primary productivity, including arguments for elevated (e.g., Algeo et al., 2013; Georgiev et al., 2015; Meyer et al., 2011; Suzuki et al., 1998) versus suppressed primary production (e.g., Grasby et al., 2016, 2020; Knies et al., 2013; Twitchett, 2001). For example, a vigorous biological pump was proposed by Meyer et al. (2011), while other suggested uppression of primary production under nutrient limitation (Grasby et al., 2016; Schobben et al., 2020). Marine primary production during the Permian and Triassic was dominated by algae, especially green algae (Payne and van de Schootbrugge, 2007). A near-total dominance of (cyano)bacterial primary production has been invoked across and/or after the mass extinction, based on the high abundance of 2-methylhopane biomarkers (Cao et al., 2002; Jia et al., 2012; Xie et al., 2005, 2017), although the link between 2-methylhopanes and cyanobacteria is now debated (Naafs et al., 2022; Welander et al., 2010), as well as the widespread proliferation of cyanobacterial microbialites (e.g., Ezaki et al., 2003; Foster et al., 2020; Wu et al., 2014; Xie et al., 2010).

The Early Triassic was a key period of algal evolution that initiated the establishment of modern marine algal assemblages (e.g., de Clerck et al., 2012; Falkowski et al., 2004). These modern algae expanded at the expense of Chl *a/b* green algae (Falkowski et al., 2004), an evolutionary step that has been reconstructed (albeit at low temporal resolution) based on changes in sterol-derived (steranes) biomarker distributions (C_{28}/C_{29} ratio; Schwark and Empt, 2006). This is supported by other data. For example, dinoflagellates emerged in the Early Triassic with the first occurrence of dinocysts (Mouradian et al., 2007) and increased abundances of triaromatic dinosteranes, biomarkers for dinoflagellates (Summons et al., 1992). Other modern algae include diatoms that first appeared in the Early Jurassic (Nakov et al., 2018) and coccolithophores that arose before the Carnian (de Vargas et al., 2007; Gardin et al., 2012). Thus, not all of these modern algae emerged and/or expanded in the Early Triassic, and they did not dominate marine plankton until the late Mesozoic (Falkowski et al., 2004). Rather, this evolutionary step of modern algal expansion has been attributed to the consequences of the EPME, which opened ecological niches and created new ecosystems, as well as the climatic conditions of the post-crisis Triassic (Falkowski et al., 2004).

Here, we explore molecular records of steranes as biomarkers for eukaryotic algae and hopanes as biomarkers for bacteria (Huang and Meinschein, 1979; Moldowan et al., 1985; Volkman, 1986, 2005) to investigate post-EPME ecological changes in ecosystem trophic foundations. We develop a long-term record of sterane distributions (C_{28}/C_{29} ratios; Schwark and Empt, 2006) and sterane to hopane [S/(S+H)] ratios from the Boreal Sea, in sections from the Sverdrup Basin in Arctic Canada that extends from the latest Permian to the earliest Middle Triassic (Anisian). This boreal record is complemented by a tropical record across the Permian/Triassic Boundary (PTB) from a section at Xiakou, South China. By extending these records to global sites using published data, we then test the hypothesis that the Early Triassic was a protracted interval of suppressed primary productivity and the turning point in algal community evolution.

2. Geological settings

We generated two novel biomarker records. The first is from the Sverdrup Basin, Arctic Canada (Bond et al., 2020; Grasby and Beauchamp, 2008, 2009; Grasby et al., 2026; Knies et al., 2013; Wignall et al., 2020b), and the second is from Xiakou [or Daxiakou as in Zhang et al., 2009], South China (Shen et al., 2016; Sun et al., 2019; Zhang et al., 2021). Both sites were previously described, logged, and characterized geochemically. We integrate these new records with previously published Boreal S/(S+H) data from Kap Stosch in East Greenland (Hays et al., 2012) and a tropical record from Meishan, South China (Cao et al., 2009) along with C_{28}/C_{29} ratios from sections in South China, including Meishan (Cao et al., 2009) and Chaohu (Saito et al., 2016).

2.1. Study sections

2.1.1. Sverdrup Basin, Arctic Canada

The Sverdrup Basin, located in the Canadian High Arctic, lay at a mid-palaeolatitude setting on the northwestern margin of Pangea during the Permian and Triassic (Fig. 1***a***). The strata in the Sverdrup Basin were deposited on a generally deep-water ramp in the latest Permian (Beauchamp et al., 2009; Embry and Beauchamp, 2019; Embry, 1989), but during the Early Triassic, conditions ranged from fluvial plain to offshore basin (Beauchamp et al., 2009; Embry and Beauchamp, 2019; Embry, 1989).

Our composite section from the Sverdrup Basin is composed of sections from Borup Fiord (N81°00′33.4″, W 81°30′51.0″), Griesbach Creek (N80°54′27.8″, W89°11′34.3″) and Spath Creek-Cape St. Andrews (N80°55′4.3″, W89°14′29.5″) (Figs. 1***b***; **S1**; Bond et al., 2020; Grasby et al., 2026; Wignall et al., 2020b), located in the northern part of the basin. It broadly represents an outer shelf setting (Fig. 1***b***; Bond et al., 2020; Wignall et al., 2020b). The Borup Fiord section starts from the middle Permian Capitanian and extends to the Spathian, from which our succession comprises 15 samples for the Permian strata (Bond et al., 2020; Grasby and Beauchamp, 2008). The 12 samples from Griesbach Creek cover the basal 50 m of the Griesbachian in our profile. Above these, 35 samples from the Spath Creek-Cape St. Andrews section (Wignall et al., 2020b), extend from around 80 m in our profile up through the Dienerian to the earliest Middle Triassic (Anisian), with two unlogged horizons that are poorly exposed from the early Smithian (Wignall et al., 2020b). The chemostratigraphy ($\delta^{13}C_{org}$) of the succession (**Fig. S1**) is well established (Grasby et al., 2026; Wignall et al., 2020b) and the sedimentary log and ichnofabrics have been previously reported (Bond et al., 2020; Wignall et al., 2020b).

2.1.2. Xiakou, South China

The Xiakou outcrop, or Daxiakou in some literature (e.g., Gao et al., 2013; Zhang et al., 2009; Zhao et al., 2013), is in Xinshan, Western Hubei, China (N31°06′52.4″, E110°48′12.5″; Shen et al., 2016). It exposes continuous stratigraphy from the latest Permian to the Dienerian, constrained by a well-established biostratigraphy via conodont, ammonoid and bivalve biozones (Zhao et al., 2013, 2015, 2019; Wu et al., 2012). During the Permo-Triassic transition, Xiakou was in the centre of the Yangtze Platform, within the South China Block (Fig. 1***c***). This tropical area lay in the eastern Paleo-Tethys (Fig. 1***a***), representing a deep-water offshore setting (Lei et al., 2017; Shen et al., 2016; Sun et al., 2019). No long-term $\delta^{13}C_{org}$ record (Zhang et al., 2021) is available for the section but a published $\delta^{13}C_{carb}$ record (Sun et al., 2019) spans our biomarker profile, aiding the biostratigraphy for our correlation (**Fig. S1**). Among the 16 samples we analysed from Xiakou, only two are from the latest Permian, and the rest were are from the Early Triassic, with the uppermost samples likely of early Smithian age (Wu et al., 2012; Zhao et al., 2013, 2015, 2019).

2.2. Previously published sections

2.2.1. Kap Stosch, East Greenland

During the Permo-Triassic interval, the Kap Stosch section was deposited on a deep-water ramp on the margin of the Boreal Sea in northwestern Pangea (Fig. 1***a***; Sanson-Barrera et al., 2015; Shen et al., 2016). The EPME has been identified via fossil assemblages (Sanson-Barrera et al., 2015; Schneebeli-Hermann et al., 2017; Twitchett et al.,

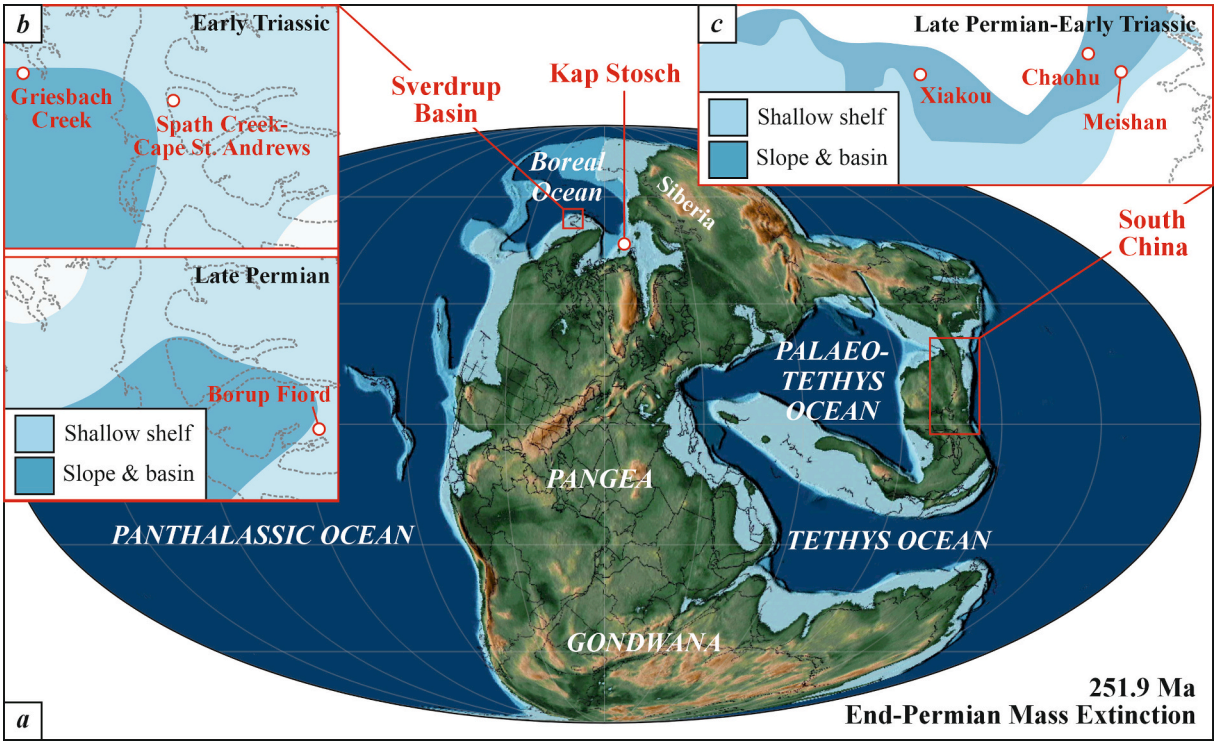

Fig. 1. The palaeolocations around end-Permian mass extinction for the sites mentioned in this manuscript.
The figure presents (***a***) the palaolocations of Sverdrup Basin, Kap Stosch and South China Block, and the inset (***b***) represents the detailed palaeolocations of the Xiakou, Chaohu, and Meishan sections in the South China Block, and inset (***c***) represents the palaeolocations of sections in Sverdrup Basin, Arctic Canada. The palaeomap of the globe is based on Scotese (2014). The palaeogeography for the South China Block and the Sverdrup Basin is modifed from Feng et al. (1997) and Beauchamp and Grasby (2012), respectively.

2001). The section spans from the latest Permian to the earliest Griesbachian (Hays et al., 2012) with a notable Changhsingian unconformity (Twitchett et al., 2001). Here, we utilise previously published S/(S+H) profiles (Hays et al., 2012) focusing on the EPME interval and immediately overlying sediments. No published C_{28}/C_{29} records are available for this section.

2.2.2. Meishan, South China

The Global Stratotype Section and Point for the base of the Triassic is located at Meishan, a section located on the Yangtze Platform of the South China block (Fig. 1***b***; Yin et al., 2001). This section was deposited in a deep-water setting, transitional from platform to slope through the Permian and Triassic (Yin et al., 2001). The age and stratigraphy of Meishan are well established through extensive zircon and sanidine dating (Burgess et al., 2017) and several high-resolution organic and inorganic stable carbon isotope records (Cao et al., 2002; Huang et al., 2007; Luo et al., 2010; Shen et al., 2011; Wang et al., 2005; Xie et al., 2007). The specific section analysed by Cao et al. (2009) is Meishan Core-1 from a borehole drilled ~550 m west of the original Meishan section. Here we recalculated the published data from Cao et al. (2009) and compiled them into S/(S+H) and C_{28}/C_{29} records extending from the late Wuchiapingian to the early Dienerian.

2.2.3. Chaohu, South China

Chaohu is another section from the Yangtze Platform in the South China block that was generally deposited in deep water (Fig. 1***b***; Chen et al., 2011; Saito et al., 2016; Yang et al., 2011). High-resolution correlation of conodont and ammonoid zones is available (Tong and Zhao, 2011; Zhao et al., 2008), alongside a detailed description of ichnotaxa (Chen et al., 2011). Published inorganic and organic stable carbon isotope profiles (Du et al., 2021) allow integration of previously published Early Triassic C_{28}/C_{29} ratios from this site (Saito et al., 2016) with our new data. No hopane data are available for this section, precluding determination of S/(S+H) ratios.

3. Approach

3.1. Experimental methods for biomarker reconstructions

3.1.1. Extraction and separation

All organic analyses were performed at the Organic Geochemistry Unit (OGU), University of Bristol. Weathered surfaces of original rock samples were removed before the samples were crushed into fragments (<1 cm^3). The fragments were agitated in an ultrasonic bath in dichloromethane:methanol (DCM:MeOH) (9:1 *v*/v) for 5 min to remove potential contaminants. The fragments were then ground to fine powders in a ball mill at 500 rpm for 5 min. Low-ion sand (3 min, 500 rpm) and ethanol were used to clean the ball mill between samples to avoid cross contamination.

Lipids were extracted from powdered rock (~30 g) using a Soxhlet apparatus with a DCM:MeOH (2:1 v/v, 200 mL) azeotrope for 48 h. An internal standard (5α-androstane) was added to the sediment prior to extraction. Total lipid extracts (TLEs) were concentrated through a Turbovap device under a gentle N_2 flow at 40 °C. Half of the TLE was separated using silica open column chromatography into saturated, aromatic, and polar fractions successively by 3 mL of hexane, 4 mL of hexane:DCM (3:1 v/v) and 4 mL of DCM: MeOH (1:2 v/v).

3.1.2. GC-MS

Saturated fractions were dried under a gentle N_2 flow and dissolved in ethyl acetate before analysis with a Thermo ISQ gas chromatography–mass spectrometry (GC–MS) instrument. After injection of 1 μL onto a Zebron-I non-polar column (50 m × 0.32 mm × 0.10 μm), the GC oven was heated from 70 °C (held for 1 min) to 130 °C at 20 °C/min,

then to 300 °C (held for 25 min) at 4 °C/min. The mass spectrometer continuously scanned between *m/z* 50 and 650. Biomarkers were identified and quantified based on published spectra and retention times: steranes (Wang and Fingas, 1995) and diasteranes (Peters et al., 2014) were identified and quantified using the *m/z* 217 fragment; hopanes were identified and quantified using the *m/z* 191 fragment (Wang and Fingas, 1995).

3.2. Biomarker proxies

Steranes and hopanes are classes of cyclic triterpenoids. Steranes, the diagenetic products of sterols, are nearly exclusively synthesized by eukaryotes via the oxygenated pathways of sterol synthases (Barton et al., 1975; Belin et al., 2018; Volkman, 2003, 2005), although a limited number of bacteria are known to make sterols (Hoshino and Gaucher, 2021; Pearson et al., 2003). As such, they are biomarkers for eukaryotes, inferred in non-marginal marine settings to be predominantly derived from eukaryotic algae, especially algal photoautotrophs, although they can have a range of sources given their biological ubiquity. Hopanes, derived from bacteriohopanepolyols and diploptene/diploterol, appear to be bacterial analogues to eukaryotic sterols (Sáenz et al., 2015). Sharing a common squalene precursor with sterols, hopanoids are nearly exclusively synthesized by bacteria to either C_{30} diplopterol or diploptene and then extended into the C_{35}-bacteriohopanepolyol-like core structure (Ourisson et al., 1979, 1987; Rohmer et al., 1984). These hopanoids are then diagenetically and catagenetically transformed into C_{27} to C_{35} hopanes.

$$\frac{S}{S+H}=\frac{\sum sterane\ (m/z\ 217)+\sum diasterane\ (m/z\ 217)}{\sum sterane\ (m/z\ 217)+\sum diasterane\ (m/z\ 217)+\sum hopane\ (m/z\ 191)},$$

Although an internal standard (5α-androstane) was added, we have not converted peak areas to true concentrations given the variation in response factors, especially among hopane isomers, which would be further impacted by differences in thermal maturity between sections. The *m/z* 217 to TIC response factors differ between steranes and diasteranes, introducing minor differences when converting to true concentrations. Therefore, relative abundances are present here to track changing trends. Abundances, normalised to nC$_{18}$-alkanes, are also included to explore the potential influence from lithological changes and/or preservation variability.

We also calculate sterane to hopane [S/(S+H)] ratios and sterane distributions (C_{28}/C_{29} ratios) to reconstruct past changes in algal productivity and ecology. Both must be interpreted with caution. Sterols are produced by all eukaryotes and a very limited group of bacteria. The C_{27} sterols are abundant in animal heterotrophs, including zooplankton and metazoans (e.g., Idle and Wisman, 1971). The C_{29} (and to a lesser degree, C_{28}) sterols are also abundant in higher plants (Nes, 1977; Volkman, 1986, 2005), although our sites appear to be dominated by marine organic matter inputs based on the overall biomarker distributions. Similarly, hopanes derive from a variety of bacteria, including cyanobacteria (Collister et al., 1992; Simonin et al., 1992, 1996; Summons et al., 1999; Welander et al., 2010). As such, the S/(S+H) ratio cannot be interpreted strictly as an algal productivity proxy, especially given the likely importance of cyanobacterial production at the EPME and its aftermath (Wu et al., 2014; Xie et al., 2005, 2010). Aerobic sedimentary reworking can also impact biomarker ratios (Bobrovskiy et al., 2024). Additional caveats that apply to the specific indices are discussed below.

3.2.1. (Dia)Sterane to hopane ratios

The ratio of steranes to hopanes [S/(S+H)] (Moldowan et al., 1985) has been commonly applied as an indicator of relative eukaryotic/bacterial biomass (Belin et al., 2018; Sáenz et al., 2012; Sepúlveda et al., 2009). Given the sources of steranes and hopane in marine settings, where terrestrial plant inputs are minimal, the ratio largely reflects the relative abundances of eukaryotic algal over heterotrophic/(cyano) bacterial inputs, and therefore eukaryotic primary production variations. In conditions where cyanobacteria play a minor role, the ratio represents algal over heterotrophic bacteria and qualitatively changes in total primary production.

However, analytical caveats can arise via the thermal and diagenetic rearrangement of steranes into diasteranes (Rubinstein et al., 1975). In our sections, in particular in the Sverdrup Basin, diasteranes are abundant. Similar but less abundant, diasteranes were observed in Xiakou (this study), and reported in the Kap Stosch (Hays et al., 2012), Meishan (Cao et al., 2009) and Chaohu sections (Saito et al., 2016). To best represent source change and align our newly measured data with that from the literatures, we modified the S/(S+H) ratios by including diasteranes. This is essential because the relative abundance of diasteranes and steranes varies significantly through the section, likely due to differences in lithology (Riolo et al., 1986). Our S/(S+H) ratios, therefore, are expressed as below:

where the steranes include C_{27}–C_{29} regular steranes with 5α,14α,17α (20S+20R) and 5α,14β,17β (20S+20R) isomers (Moldowan et al., 1985), and the diasteranes include both the 13β,17α (20S+20R) and 13α,17β (20S+20R) isomers. For the hopanes, the calculations encompass all C_{29}–C_{35} components, with both the 22S and 22R epimers for the C_{31}–C_{35} homologues (Moldowan et al., 1985); we note, however, that the abundances of $C_{>32}$ homohopanes are near the detection limits in the Sverdrup Basin succession. Previously published S/(S+H) ratios appear to have been generated using the same approach but vary in the specific compounds included. For example, Cao et al. (2009) also included C_{30} steranes and C_{27}–C_{28} hopanes. To be consistent, we revised the Meishan S/(S+H) ratios from Cao et al. (2009) to exclude the C_{30} steranes. Unfortunately, the data were not available to recalculate their ratios without the C_{27} and C_{28} hopanes. Although this will shift the Meishan S/(S+H) ratios towards slightly lower values, this has only a minor impact on the ratios given the relatively low abundances of these short-chain components.

The biomarkers were integrated using *m/z* 217 (sterane and diasterane) and 191 (hopane) mass chromatograms, respectively. The specific abundance of *m/z* 217 and 191 in isomers of (dia)steranes and hopanes depends on thermal maturity, which differs among the sections, so that the variant response factors discussed above could introduce minor differences in S/(S+H) ratios among sections. Therefore, the ratios are reported in their traditional forms based on the respective mass chromatograms and are not true concentration ratios; we have included all C_{27}–C_{29} (dia)steranes and C_{29}–C_{35} hopanes; and we avoid comparing absolute values of S/(S+H) ratios among sections, focussing on trends instead.

3.2.2. C_{28}/C_{29} sterane ratio

The distributions of algal (4-desmethyl) sterols differ among major groups, such that the (4-desmethyl) sterane distributions can be used to reconstruct the dominant algal community. Red algae preferentially produce C_{27} relative to the C_{28} and C_{29} sterols (e.g., Kodner et al., 2008; Nes, 2011; Volkman, 2005). Other algal groups preferentially produce C_{28} and C_{29} sterols. The algal groups prevailing in the modern ocean (e.g., dinoflagellates, diatoms and coccolithophores), usually the Chl *a*/*c*

users, synthesize predominantly C_{28} sterols over the C_{29} components (Haubrich et al., 2015; Knoll et al., 2007b; Nes, 2003; Rampen et al., 2010). Green algae including *Chlorophyceae* and *Charophyceae* are almost all Chl *a*/*b* users and synthesize relatively abundant C_{29} sterols (Kodner et al., 2008; Nes, 1977, 2000; Volkman, 1986; Volkman and Maxwell, 1986). Nevertheless, a noteworthy exception is the *Prasinophyceae*, which is frequently referred to as "disaster taxa" in the Early Triassic. This group preferentially produces C_{28} over C_{29} sterols (Kodner et al., 2008; Volkman, 2005). Hence, despite significant variance of sterol distributions among species, proportions of C_{27}, C_{28} and C_{29} steranes have been used to reconstruct changes in algal community structure, both over long timescales to explore algal evolution (Grantham and Wakefield, 1988; Knoll et al., 2007b) and across biotic crises such as the Cretaceous-Paleogene Mass Extinction (Sepúlveda et al., 2009; Sosa-Montes de Oca et al., 2023), the EPME (e.g., Saito et al., 2016), and Oceanic Anoxic Event (OAE) 2 (e.g., Forkner et al., 2021). Such interpretations require caution, as the sterol source assessment reflects only general trends rather than diagnostic signatures (e.g., Nes, 2011; Volkman, 2005), and they can also be influenced by diagenetic and catagenetic processes.

Here, we focus on the proportion of C_{28} relative to the C_{29} steranes as a tracer for changes in algal communities (Schwark and Empt, 2006). Our C_{27} components are partially obscured by co-eluting C_{29} diasteranes and are therefore excluded from our analysis and interpretation. Thermal maturity can impact the C_{28} and C_{29} compounds, and the ratio exhibits consistency with their rearranged products (C_{28}/C_{29} diasteranes; Peters et al., 2004). Nonetheless, the C_{28} steranes are relatively susceptible to microbial degradation compared to the C_{29} components such that the original signals would be obscured under intense biodegradation (e.g. Seifert and Moldowan, 1979; Peters et al., 2004).

4. Results

4.1. Thermal maturity proxies

In the samples from the Sverdrup Basin sections, the regular steranes are characterized by a slight dominance of 5α,14α,17α over 5α,14β,17β stereoisomers, but this varies among samples (**Fig. S3*a***). Diasteranes are present as 13β,17α and 13α,17β isomers with varying abundances relative to the regular steranes (**Fig. S3*a***). The hopanes show a thermally mature distribution, characterized by a lack of 17β(H),21α isomers (**Fig. S3*b***) and C_{32} 22S/(22S+22R) ratio (Seifert and Moldowan, 1980) that ranges from 0.3 to 0.7 (average ~0.6). The thermally mature distribution is consistent with C_{29} sterane $\beta\beta/(\beta\beta+\alpha\alpha)$ ratios between 0.4 and 0.6, and C_{29} 20S/(20S+20R) ratios (Mackenzie, 1984) between 0.2 and 0.7 (**Fig. S2**). These data all suggest that the organic matter is mature with respect to oil generation, with many ratios having reached their thermal equilibrium distribution (**Fig. S2**; Mackenzie et al., 1980; Peters and Moldowan, 1991; Seifert and Moldowan, 1980). Thid interpretation is also consistent with phytane/nC$_{18}$ ratios being comparable,

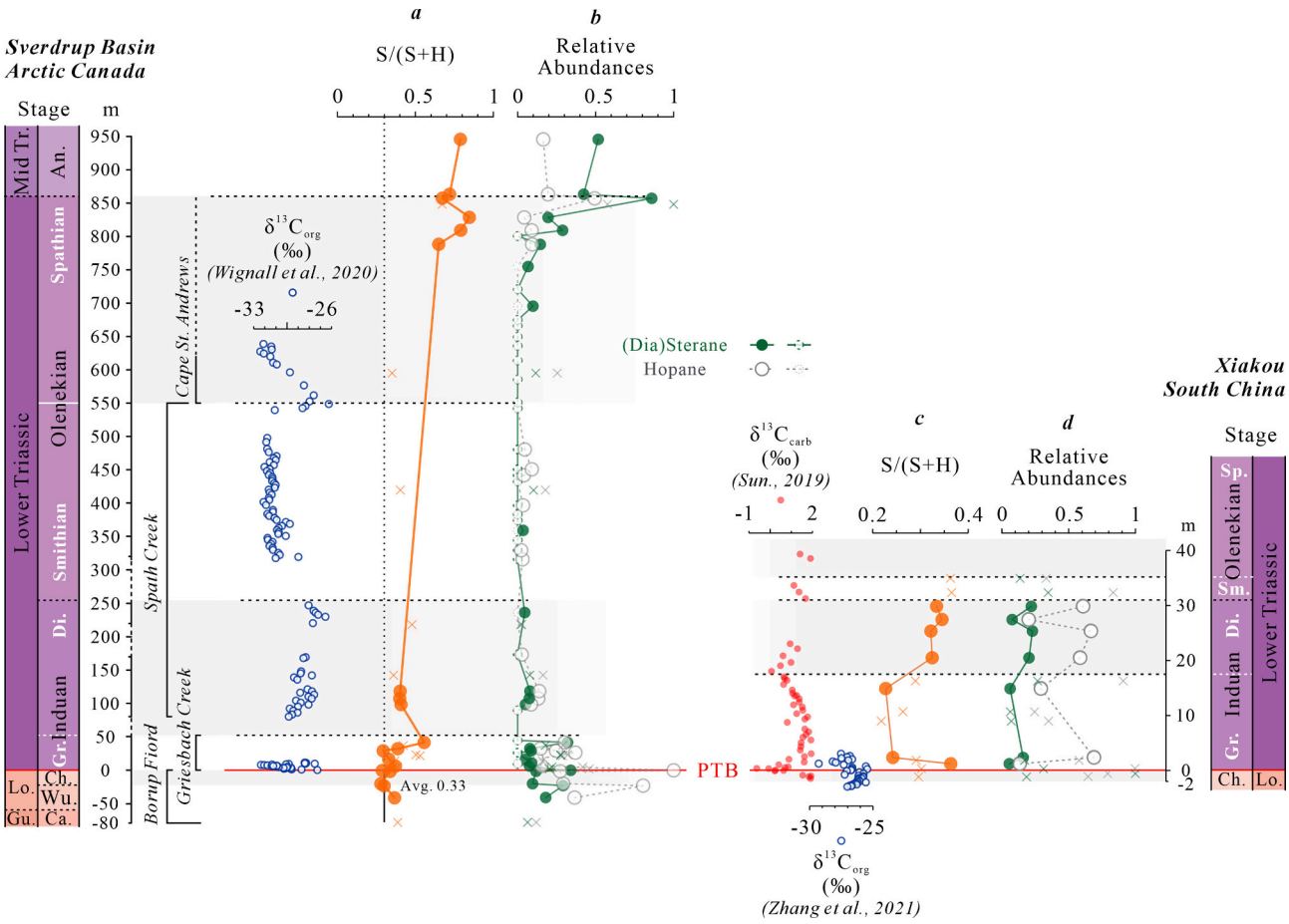

Fig. 2. Stratigraphic, geochemical and biomarker data of the study sites.
The figure presents (***a***, ***c***) S/(S+H) ratios and (***b***, ***d***) sterane (including diasterane) and hopane abundances (normalized to highest abundance in section) from the composite section in the Sverdrup Basin, Arctic Canada (left) and Xiakou, South China (right). The cross symbols represent samples high in thermal maturation (**Fig. S2**), and the abundances are untrustworthy. The $\delta^{13}C_{org}$ data of Sverdrup Basin are from Wignall et al. (2020b); the $\delta^{13}C_{org}$ and $\delta^{13}C_{carb}$ data of Xiakou are from Zhang et al. (2021) and Sun et al. (2019), respectively. The orange line denotes the Permo-Triassic boundary (PTB). Gu.: Guadalupian; Lo.: Lopingian; Mid Tr.: Middle Triassic; Ca.: Capitanian; Wu.: Wuchiapingian; Ch.: Changhsingian; Gr.: Griesbachian; Di.: Dienerian; Sm.: Smithian; Sp.: Spathian; An.: Anisian.

~0.3, throughout the Borup Fiord, the Griesbach Creek and the Spath Creek samples; however, they are much higher, ~1.2, within parts of the Cape St. Andrews section between 640 and 730 m, suggesting a different diagenetic history (**Fig. S2*a***; e.g., Pirnik et al., 1974).

Our biomarker data for thermal maturation complement published vitrinite reflectance and Rock-Eval T_{max} data, together indicating that the Borup Fiord, the Griesbach Creek and the Spath Creek have progressed into the late oil to gas generation window and are higher in maturation than the Cape St. Andrews section (Dewing and Obermajer, 2011; Galloway et al., 2018). As discussed above, the lower thermal maturity at the Cape St. Andrews section, representing the mid Spathian, could impact S/(S+H) trend of the Sverdrup Basin and this is considered in our subsequent discussion.

The biomarkers and isomerization are similar in Xiakou. The C_{32} hopane 22S/(22S+22R) ratio ranges from 0.5 to 0.7, consistent with C_{29} $\beta\beta/(\beta\beta+\alpha\alpha)$ (0.5–0.7) and C_{29} 20S/(20S+20R) (0.4–0.8) sterane ratios (**Figs. S2, S4**). The Xiakou succession is close to the margin of the oil window and presents stable thermal maturity throughout, suggesting robust stratigraphic trends of sterane and hopane proxies. The phytane/nC_{18} ratios maximize at the PTB, suggesting enhanced microbial degradation (Pirnik et al., 1974). In the overlying Early Triassic, the ratios are variable (**Fig. S2**), likely due to changes in lithologies (Peters et al., 2004) as shales are interbedded with limestones (Shen et al., 2016; Sun et al., 2019).

4.2. Relative abundances of (dia)steranes and hopanes

In the Sverdrup Basin, abundances of (dia)steranes and hopanes increase from the middle to late Permian, peaking in the late Permian (Fig. 2***b***). Abundances in the earliest Griesbachian samples are similar to those recorded in Permian samples, lower than the pronounced peak at around PTB (Fig. 2***b***), although we note that this represents a comparison of samples from two sections in our composite record. The abundances at Xiakou through the latest Permian into the PTB (Fig. 2***d***), although diagenesis could obscure the original levels. In the Griesbachian, abundances decrease and then become stable (Fig. 2***d***).

On a longer timescale, abundances of (dia)steranes and hopanes in the Sverdrup Basin decrease dramatically from the middle Dienerian, and then maintain these low values until the late Spathian (Fig. 2***b***). This is probably not due to the different thermal maturation of the composite sections, which instead would result in higher abundances in the less mature Spath Creek-Cape St. Andrews (Dewing and Obermajer, 2011). In the late Spathian–earliest Anisian interval (dia)steranes and hopanes in the Sverdrup Basin rebound to abundances comparable to those in the Permian (Fig. 2***b***). In contrast, (dia)sterane and hopane abundances at Xiakou increase since the late Griesbachian and the high values persist through the Dienerian and into the early Smithian (Fig. 2***d***).

Caution is required in these interpretations, because somewhat different trends emerge in nC_{18}-normalised abundances of (dia)steranes and hopanes. In the Sverdrup Basin, the normalised abundances follow the non-normalised trends, except for the late Spathian where they are low. At Xiakou, nC_{18}-normalised abundances exhibit trends opposite to those of the non-normalised biomarkers, suggesting at least some of the variation in the latter could be due to organic matter preservation (**Fig. S5*d***).

4.3. Sterane to hopane ratios

From the middle to late Permian, the S/(S+H) ratios from the Sverdrup Basin (Figs. 2***a***, 3***c***) and the single datum from Xiakou (Figs. 2***c***, 3***d***) are ~0.3. At Meishan, where higher resolution records have been obtained, ratios are similar but more variable (0.1–0.35) with highest values occurring during the Wuchiapingian/Changhsingian transition and the latest Changhsingian (Fig. 3***b***). The Kap Stosch section, which spans the latest Changhsingian, is characterized by an increasing trend, from a low value similar to those of other sites (~0.3), to a maximum of ~0.8 just below the Permo-Triassic unconformity (Fig. 3***a***).

Following the PTB in the Sverdrup Basin, the S/(S+H) ratios are

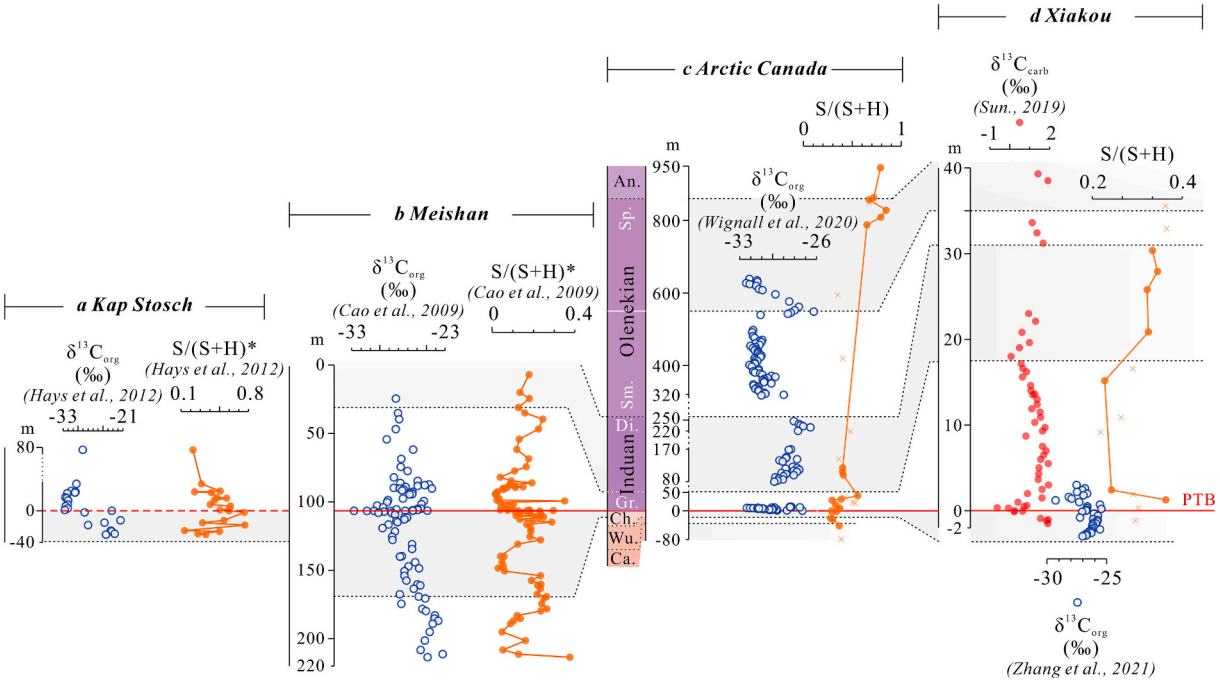

Fig. 3. $\delta^{13}C$ records and S/(S+H) ratios for the study sites and published sections mentioned in this manuscript.
The figure includes datasets from (***a***) Kap Stosch, East Greenland, (***b***) Meishan, South China, (***c***) Sverdrup Basin, Arctic Canada and (***d***) Xiakou, South China during the Late Permian–Early Triassic interval. The cross symbols represent samples high in thermal maturation (**Fig. S2**), and the abundances are untrustworthy. Note that at Kap Stosch and Meishan S/(S+H) ratios were calculated using different steranes and hopanes, precluding comparison of absolute values (see text). The orange line denotes the Permo-Triassic boundary (PTB). Ca.: Capitanian; Wu.: Wuchiapingian; Ch.: Changhsingian; Gr.: Griesbachian; Di.: Dienerian; Sm.: Smithian; Sp.: Spathian; An.: Anisian.

similar to or higher than the value averaged from the Wuchiapingian-Changhsingian strata (Figs. 2***a***, 3***c***). Ratios then increase to >0.5 in the later Griesbachian. At Xiakou, the ratios decrease during the earliest Triassic but increase in the later Griesbachian into the Dienerian (Figs. 2***c***, 3***d***). In contrast, S/(S+H) ratios in the Kap Stosch and Meishan sections decrease into the earliest Griesbachian from their maxima at the EPME (Figs. 3***a***, ***b***). Although the data from the Sverdrup Basin are sparse, they provide no evidence for a decrease in S/(S+H) ratios following the EPME.

Our Sverdrup Basin data are the first S/(S+H) record throughout the Early Triassic, albeit with gaps due to low biomarker abundances. The record documents an increase in the S/(S+H) ratio from a value of ~0.3 to ~0.4 through the early Dienerian (Figs. 2***a***, 3***c***). Given the low abundances of steranes and hopanes in our samples, we are reluctant to over-interpret variations based on a single datum, but the long-term trend is robust, culminating in high values, ranging from 0.6 to 0.8, in the uppermost Spathian and Anisian intervals. The Xiakou section only extends into the earliest Smithian, but it also records a rise in S/(S+H) ratios (from ~0.2 to 0.35) following the EPME (Figs. 2***c***, 3***d***).

4.4. C_{28}/C_{29} sterane ratios

During the pre-EPME Permian, the C_{28}/C_{29} ratios from the Sverdrup Basin (~0.6) and the two samples from Xiakou (~0.8) are low, although our sampling resolution is also low compared to the Early Triassic sediments (Fig. 4***a***). Meishan presents values between 0.2 and 0.4, while there are no available data from Chaohu for the late Permian. Thus, our compiled late Permian C_{28}/C_{29} ratios are ~0.4 (ranging from 0.2 to 0.8). Although our data are dominated by those from Meishan, all sites have relatively low values.

Relative to the late Permian, C_{28}/C_{29} ratios of the Early Triassic increase, although the trends differ among sections. In the Sverdrup Basin, ratios increase from pre-EPME values of ~0.6 to ~0.8 in the earliest Griesbachian. In contrast, no obvious change is observed at Xiakou (by ~0.1). Any change in this section could have been smoothed by enhanced biodegradation around the PTB which preferentially degraded the C_{28} steranes (e.g. Peters et al., 2004; Seifert and Moldowan, 1979) (also associated with the highest phytane/nC_{18} ratios, **Fig. S2*e***). In Meishan, they increase from ~0.3 in the Changshingian to ~0.7 in the earliest Griesbachian. Although Xiakou and Chaohu lack Permian records, ratios from the earliest Triassic are generally high, being above the average ~0.4 for the late Permian.

On longer timescales, C_{28}/C_{29} ratios from the Sverdrup Basin and Chaohu both record a maximum during the Dienerian, with values up to 1.3, and they remain high until the Smithian/Spathian boundary (SSB). We lack data for most of the Spathian from the Sverdrup Basin due to low sterane abundances during this interval, but even higher values (average ~1.0, from 0.7 to 1.5) occur in the upper the late Spathian-Anisian strata. At Chaohu, C_{28}/C_{29} sterane ratios decrease in the Spathian, to ~0.3. They then increase to values ranging from 0.6 to 1.4 during the latest Spathian and Anisian.

5. Discussion

5.1. Variable productivity in post-crisis Griesbachian successions

The latest Permian interval is characterized by relatively low sterane to hopane [S/(S+H)] ratios and a dominance of C_{29} over C_{28} steranes,

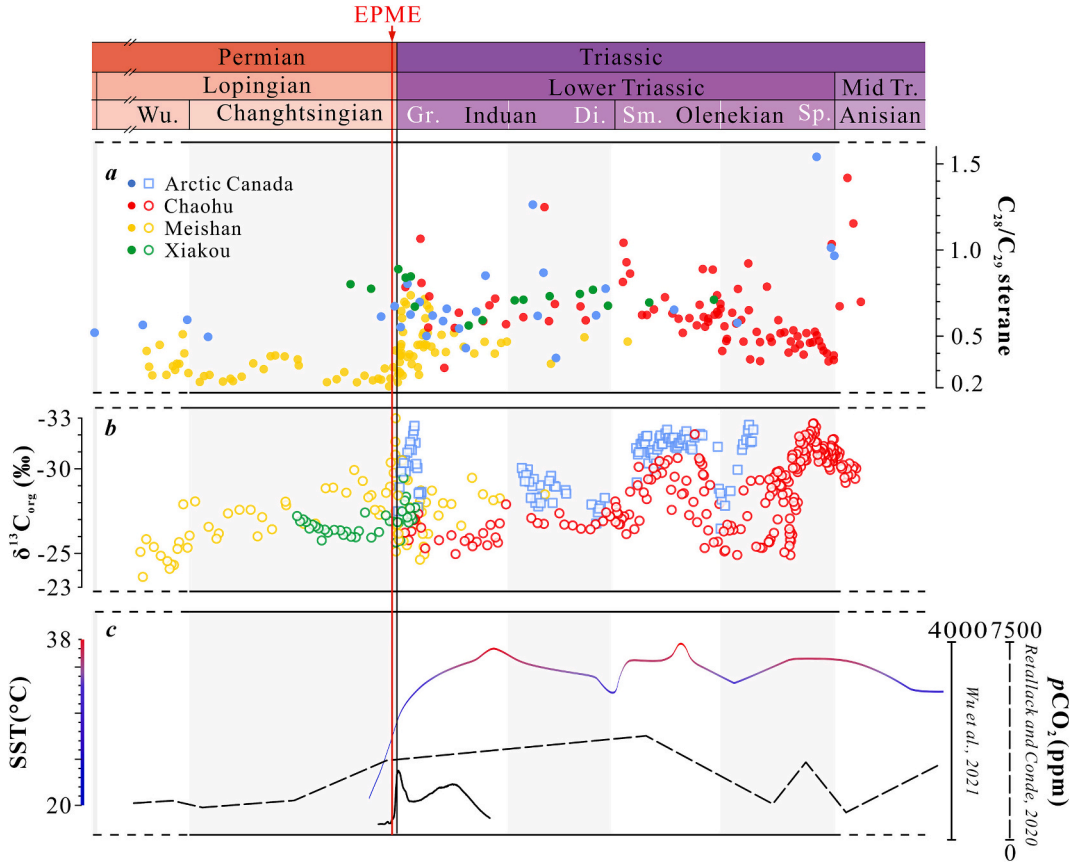

Fig. 4. Sterane C_{28}/C_{29} ratios (***a***) compiled with climate indicators [(***b***) $\delta^{13}C_{org}$, (***c***) pCO_2 (Retallack and Conde, 2020; Wu et al., 2021), and $\delta^{18}O_{apetite}$–surface sea temperatures (Sun et al., 2012)] through the late Permian and early Triassic.
Cm: Cambrian; O: Ordovician; S: Silurian; D: Devonian; C: Carboniferous; P: Permian; Tr: Triassic; J: Jurassic; K: Cretaceous; Pg: Paleogene; N: Neogene; Q: Quaternary; Wu.: Wuchiapingian; Gr.: Griesbachian; Di.: Dienerian; Sm.: Smithian; Sp.: Spathian; Mid Tr.: Middle Triassic.

especially in the Sverdrup Basin (C_{28}/C_{29} ratio of ~0.6). These data indicate low eukaryotic (algal) over bacterial production and a phytoplankton structure dominated by cyanobacteria and green algae. This is consistent with negative bulk $\delta^{15}N$ values observed in the Sverdrup Basin that indicate a high abundance of (N-fixing cyanobacterial) diazotrophy (Grasby et al., 2016; Knies et al., 2013). Reworked pollen and spores have been reported in the Middle Permian Roadian and Wordian strata as well as the Early Triassic Griesbachian (Utting et al., 2004), which could yield high proportions of C_{29} steranes via this external contribution from higher plants (Isaksen, 1995). Despite no palynological evidence suggesting similar contributions to latest Permian strata (Utting et al., 2004), we cannot exclude terrestrial input due to the regression–transgression across the Permo-Triassic transition (Embry and Beauchamp, 2019).

Collectively, we do not observe a general decrease in S/(S+H) ratios from the Permian to the earliest Griesbachian (Fig. 3). Acknowledging the low resolution, it suggests no declined in S/(S+H) across the EPME. This observation contrasts with previous claims for a global collapse in eukaryotic phytoplankton in the post-EPME oceans (e.g., Knoll et al., 2007a; Payne and van de Schootbrugge, 2007; Tappan, 1970; Twitchett, 2001). In detail, an abrupt decline across the EPME is not observed in the Sverdrup Basin (Figs. 2***a***, 3***c***) and the Meishan and Kap Stosch sections document only transient S/(S+H) declines across the EPME, the former quickly rebounding to pre-EPME levels (Fig. 3***a***, ***b***).

The relatively stable S/(S+H) ratios observed in the Sverdrup Basin suggest similar levels of algal production in the earliest Griesbachian compared to the late Permian. Note that other proxies, including TOC contents and nutrient concentrations (N, P), suggest a declined in primary production at the EPME in the Boreal Realm (Grasby et al., 2016, 2020; Knies et al., 2013). This contrast might be due to our lower resolution S/(S+H) dataset across the EPME horizon. Our S/(S+H) ratios, therefore, suggest that the impact of the EPME on phytoplankton communities was minimal, or at least transient in the Sverdrup Basin. Alternatively, it could indicate consistent productivity during an algal reorganization, since the previously inferred phytoplankton collapse was also accompanied by widespread “disaster taxa” comprising acritarchs and prasinophytes in a restructured post-EPME algal community (Algeo et al., 2011; Payne and van de Schootbrugge, 2007; Tappan, 1970; van Soelen and Kürschner, 2018). This is explored using C_{28}/C_{29} sterane distributions below.

The relative stability of the S/(S+H) ratios in the Sverdrup Basin is also surprising given the likely role of cyanobacteria in post-EPME primary production. The expansion of cyanobacteria in the Permo-Triassic interval is documented by widespread cyanobacterial microbialites (Ezaki et al., 2003; Foster et al., 2020; Heindel et al., 2018; Senowbari-Daryan et al., 2006; Wu et al., 2014; Xie et al., 2010; Yang et al., 2011). This is also documented by high proportions of 2-methylhopanes (Luo et al., 2013; Xie et al., 2005, 2010), although recent research shows that 2-methylhopanes during the Phanerozoic could have been produced by other bacteria (Naafs et al., 2022; Welander et al., 2010). The cyanobacterial blooms imply suppression of eukaryotic algae given their competition for nutrients (Knoll et al., 2007a, 2007b) and the former’s tolerance of environmental stresses such as oxygen restriction (Fay, 1992) and high temperatures (Nalley et al., 2018), as well as reduced light penetration and toxic secondary metabolites once the harmful bloom built up (e.g., Paerl and Otten, 2013; Visser et al., 2016). Cyanobacteria including diazotrophic (N-fixing) species are expected to have thrived in the Permo-Triassic nitrate-depleted euxinic oceans (Grasby et al., 2016, 2020; Luo et al., 2011; Saitoh et al., 2014; Sun et al., 2019), although ammonium could also be a source for nitrogen in anoxic oceans (Higgins et al., 2012; Naafs et al., 2019). In terrestrial settings, a harmful microbial bloom with inferred cyanobacterial contribution was also reported in the Sydney Basin (Mays et al., 2021).

Thus, cyanobacteria likely acted as an additional contributor to primary production not represented by sterane abundances and likely suppressed S/(S+H) ratios, especially in the post-crisis Griesbachian oceans. In the Sverdrup Basin and Xiakou sections, 2-methylhopanes were not found (they are below or near detection limits in mass chromatograms of *m/z* 191 and 205) and cyanobacterial mocrobialites have not been reported. Nonetheless, if cyanobacteria did thrive in the Sverdrup Basin, then the sustained S/(S+H) ratios reflect similarly robust sterane contributions and presumably algal production.

This spatially heterogeneous response of S/(S+H) ratios to the EPME could reflect global variance in the algal response. Palaeogeographical variation among algal (and wider ecological) communities could have affected organic matter production and/or the biological pump, and therefore the trends in S/(S+H) ratios across different sites. Previous studies reached contradictory conclusions on the nature of post-EPME primary productivity. For example, in South China elevated productivity is inferred from several bio-elements (Ba, Ni, Cu, etc., Liu et al., 2019; Shen et al., 2014) while a collapse in productivity is inferred from element concentrations (Zn, Cu, Liao et al., 2020) and inorganic isotope data ($\delta^{114}Cd$ and $\delta^{66}Zn$, Liu et al., 2017; Zhang et al., 2018). Other studies have argued for a sustained (e.g., Ge et al., 2022; Schoepfer et al., 2013; Takahashi et al., 2009) or temporary increase in primary production, both regionally and globally (e.g., Georgiev et al., 2015; Meyer et al., 2011; Qiu et al., 2019; Schobben et al., 2015; Zhang et al., 2007).

In summary, it is likely that post-EPME primary productivity change is complex and regionally variable (Grasby et al., 2023; Shen et al., 2015).

5.2. Diminished primary producers in the Dienerian–early Spathian

In the Sverdrup Basin, (dia)sterane and hopane abundances do not decrease in the early Griesbachian but they are low from the middle Dienerian to the late Spathian (Fig. 2***b***). The low biomarker abundances in this interval are unlikely to have been a result of sedimentological or lithological change given the similarity between the relative and the $n$$C_{18}$-normalised abundances (**Fig. S5*a***). Sedimentation rates were high (Embry and Beauchamp, 2019), such that low biomarker abundances could reflect dilution, but this would also enhance preservation. The different thermal maturity among the composite sections could be an explanation; however, if that was the case, then the middle Dienerian strata (represented by the Spath Creek-Cape St. Andrews section) which is less mature (Beauchamp and Grasby, 2012; Embry and Beauchamp, 2019) should have higher rather than lower biomarker abundances. Intensified biodegradation (between ~640 and 730 m, inferred from elevated phytane/$n$$C_{18}$ ratios, **Fig. S2*a***) could have reduced biomarker abundances during the early Spathian, but it cannot readily explain the longer-term increase for the entire Sverdrup Basin record (Fig. 2***b***). If low biomarker abundances were not caused by sedimentology and/or diagenesis, then they likely indicate that following the earliest Griesbachian much of the Early Triassic in the Sverdrup Basin was characterized by low primary productivity, as previously argued by Knies et al. (2013, 2022) and Grasby et al. (2016, 2020). This could have contributed to the observed protracted recovery from the EPME (Grasby et al., 2016).

If algal communities persisted or recovered directly after the EPME but diminished later, it was likely due to environmental factors rather than being directly linked to the biotic crisis. Intense denitrification and a reduced nutrient-N inventory have been inferred from $\delta^{15}N$ values for the Sverdrup Basin from the pre-EPME to the Dienerian (Grasby et al., 2016; **Fig. S1**), and this did not recover until the SSB (Du et al., 2023, 2024; Grasby et al., 2016; Sun et al., 2019). Full recovery of the marine nitrogen cycle did not occur until the Ladinian (Knies et al., 2022). $\delta^{15}N$ records vary globally and indicate regionally diverse responses (Luo et al., 2011; Saitoh et al., 2014; Sun et al., 2019); for example, at Meishan and Xiakou, extensive denitrification appears to have ceased before the Dienerian (Sun et al., 2019), while nitrogen fixation has been proposed to be dominant in anoxic waters depleted in trace elements (Sun et al., 2019). Unlike sites from the Tethys, a perturbaed nitrogen cycle in the Sverdrup Basin appears to have persisted through ocean

stratification that slowed the vertical circulation of nutrients (Knies et al., 2022) or deoxygenation (Grasby et al., 2016) that caused nutrient sequestration (Knies et al., 2022; Sun et al., 2019). However, given the distinct deoxygenation states of the late Dienerian and the Smithian strata (Grasby et al., 2016; Wignall et al., 2020b), nutrient sequestration is unlikely to have been a long-lasting control for the Dienerian–early Spathian productivity suppression. Therefore, regional environmental records cannot explain all of the biomarker record, but they are largely consistent with respect to indicating persistent low algal and bacterial productivity in the Sverdrup Basin from the Dienerian to early Spathian, in contrast to Xiakou, which recovered from the late Griesbachian.

Alternatively or additionally, sea surface temperature could have also exerted a profound impact. Various records indicate that temperatures rose to some of the highest levels in the Phanerozoic, peaking in the tropics during the latest Griesbachian and late Smithian at even higher temperatures than at the EPME, potentially to levels lethal to certain phytoplanktonic groups (Song et al., 2019; Sun et al., 2012) and diminishing primary production. Furthermore, thermocline deepening during warming could have led to the development of nutrient traps (Grasby et al., 2016), reflected in diminished TOC contents (<0.1 %) in the late Dienerian–Smithian of Smith Creek and Festningen sections; this appears to have occurred despite cooling-induced upwelling (Grasby et al., 2020). Therefore, warming could have exacerbated and prolonged the interval of diminished primary production (Grasby et al., 2016).

The late Dienerian–Smithian appears to mark a change in biotic recovery, at least in the Sverdrup Basin, perhaps caused by a combination of water column deoxygenation, nutrient depletion and elevated temperatures. Regardless of the mechanism(s), it remains unclear why a similar dearth of biomarkers does not occur in the Dienerian in the aftermath of the EPME which was also associated with extremes of temperature (Sun et al., 2012) and nutrient depletion (Grasby et al., 2016; Knies et al., 2013, 2022; Sun et al., 2019). However, this could be an artefact of sedimentation rates, and we suggest that protracted high temperatures and nutrient limitation caused long-term suppression of primary production during the Early Triassic, at least in the Sverdrup Basin.

Following the SSB, the denitrification nutrient sink in the Sverdrup Basin reduced (Grasby et al., 2016, 2020; Sun et al., 2019), and this would have presumably facilitated a eukaryotic algal recovery (Du et al., 2021; Grasby et al., 2016; Song et al., 2019). Moreover, cooling at the SSB, inferred for example from a calcite $\delta^{18}O$ increase in South China (Sun et al., 2012), appears to have been associated with a resumption of eukaryotic primary productivity attributed to improved ocean circulation and water column oxygenation (Song et al., 2019; Sun et al., 2012). These factors are not immediately recorded by an increase in biomarker abundances, which remain low until the late Spathian (Fig. 2***f***). This could reflect a delayed response, perhaps due to the persistence of nutrient limitation indicated by low sedimentary N/P ratios (<3) (Grasby et al., 2016).

Biomarker evidence indicates that the algal recovery in the Sverdrup Basin occurred in the late Spathian–earliest Anisian (Fig. 2). Both sterane relative abundances and S/(S+H) ratios reach their highest values at this time (Fig. 2***a, b***), suggesting high algal productivity and a predominance of eukaryotes (algae) over bacteria. The nC$_{18}$-normalised abundances are decoupled from non-normalised abundances and only recover to low levels (**Fig. S5*b***). This interval is associated with elevated S/(S+H) and C_{28}/C_{29} ratios (Fig. 4***a***), indicating that the main source for the organic matter remain marine. Thus, it appears that the late Spathian-earliest Anisian was associated with enhanced algal production (and potentially preservation) as suggested by Chen and Benton (2012). The recovery co-occurs with the shift towards higher $\delta^{18}O$ values that are associated with cooling into the Middle Triassic Anisian (Sun et al., 2012; Trotter et al., 2015). Intriguingly, previous work suggests that the pre-Anisian or earliest Anisian reflects another environmental crisis. There is evidence for globally widespread marine deoxygenation, namely abundant aromatic carotenoids indicating surface-water euxinia at Chaohu (Saito et al., 2014), peaks in Mo concentrations in the Sverdrup Basin interpreted as evidence for deoxygenation (Grasby et al., 2016), as well as an acidification event (Song et al., 2021). These changes could have contributed to higher production and better biomarker preservation. Moreover, increased abundances and S/(S+H) ratios might underestimate the primary productivity given the potential contribution by cyanobacteria and/or green sulphur bacteria (although we could not detect their associated biomarkers). Thus, we suggest that in the Sverdrup Basin, eukaryotic algal production increased both absolutely and relative to bacteria around the earliest Anisian, following the long interruption during the Dienerian–Smithian.

5.3. EPME and the Early Triassic reshaping of marine algal ecosystems

Although algae produce a diverse suite of steroids, Chl *a/c* or *a/b* users preferentially produce C_{28} and C_{29} sterols, respectively, and this has been used to track algal evolution (Knoll et al., 2007b; Kodner et al., 2008; Schwark and Empt, 2006). The predominant modern Chl *a/c*-containing algae include dinoflagellates, diatoms and coccolithophores (Bachvaroff et al., 2005; de Clerck et al., 2012; Falkowski et al., 2004; Khan et al., 2020), whereas Chl *a/b*-utilizing green algae are relatively ancient (Büchel, 2020; Falkowski et al., 2004; Khan et al., 2020). Consequently, the rise of Chl *a/c* users (or modern algae) has been invoked as the main driver of the gradual Phanerozoic increase in C_{28}/C_{29} sterane ratios (Knoll et al., 2007b; Schwark and Empt, 2006). In addition to this long-term change, Schwark and Empt (2006) showed that significant fluctuations occurred in C_{28}/C_{29} ratios during major biotic crises, for example increasing from ~0.5 during the Permian to a higher value of >0.7 at the end of the Triassic, with the EPME perhaps being an important accelerator.

Our new data elaborate on these previous findings. In our dataset, C_{28}/C_{29} ratios are indeed lower in Permian sediments but the increase to higher values occurs rapidly across the PTB (Fig. 4***a***). Focusing on the Meishan section, the ratio increases by ~0.4 (from ~0.3 in the Changshingian to ~0.7 in the earliest Griesbachian), suggesting an abrupt increase in the proportion of algae that produce higher C_{28} to C_{29} sterol ratios. In the Sverdrup Basin, C_{28}/C_{29} ratios are variable during the Griesbachian–Anisian, but typically higher than in Permian intervals. In Chaohu, the C_{28}/C_{29} ratios are also high during the Smithian (Saito et al., 2016), although they decrease towards the end of the Spathian (Fig. 4***a***), which could reflect the radiation of calcareous algae (green algae species) in the South China sections (Song et al., 2011). Crucially, although C_{28}/C_{29} ratios vary among sites during the Early Triassic, they are generally high compared to the Permian values, suggesting that despite local variations, the Triassic marked a global change in algal assemblages, although the magnitude of changes differs between locations. This suggests that either Chl *a/c* algae had already expanded in the Early Triassic predating their abundant fossil records (dinocysts or coccoliths), or other algae synthesizing higher proportions of C_{28} sterols, such as the *Prasinophyceae,* became dominant as part of the post-EPME algal assemblage, as indicated by palynology in other Boreal sections (Finnmark Platform and Jameson Land; van Soelen and Kürschner, 2018).

Secondary endosymbiotic events have been invoked to explain the rise of modern algal species during the Mesozoic, including photosynthetic dinoflagellates, diatoms and coccolithophores (Grisdale and Archibald, 2017). Through loss of previously dominant plankton, the EPME may have created niches for these innovations (Falkowski et al., 2004), as might have subsequent climate/biogeochemical variations. Indeed, the C_{28}/C_{29} ratios appear to co-vary with aspects of the Early Triassic $\delta^{13}C$ record, with elevated ratios following the EPME, at the SSB and in the latest Spathian and Anisian (Fig. 4***b***). Global negative carbon isotope excursions are usually attributed to carbon cycle perturbations, and specifically the release of ^{13}C-depleted carbon and elevated pCO_2 (Cui et al., 2021; Joachimski et al., 2022; Kump, 2018; Wu et al., 2021), and dramatic temperature shifts (Grasby et al., 2020). Some intervals

likely reached temperatures towards the limits of mesophilic life, especially in tropical regions (Sun et al., 2012). Such climatic perturbations could have changed algal metabolism via photosynthesis or photoprotection. Enhanced UV radiation has also been reported based on abnormal pollens at the end of the Permian (Liu et al., 2023), and this could also suppress some algae given variant photoprotection regulation (Goss and Jakob, 2010), although it is unknown whether such conditions extended into the Early Triassic. Toxic metal stress has been suggested based on abnormal pollen (Chu et al., 2021), and this could also impact eukaryotic algae (Nowicka, 2022). Moreover, the feedbacks of pCO_2-induced warming, such as an expansion of ocean anoxia (Grasby et al., 2013; Slater et al., 2019), could have impacted algal ecology (and the sedimentary sterane record). For example, non-green algae such as Chrysophyta (preferentially producing C_{29} sterol) and Rhodophyta (preferentially producing C_{27} sterol) (Volkman and Maxwell, 1986), have a relatively lower O_2 demand compared to green algal species (Badger et al., 2000). These non-green algae could have been competitive in the poorly oxygenated environments associated with the EPME and Early Triassic, further suppressing green algae in the post-crisis oceans. Furthermore, the perturbations in the marine N-cycle and intervals of nitrate-depleted oceans could have favoured specific primary producers, for example, cyanobacterial diazotrophs (Falkowski, 1997; Villareal et al., 1993). We propose that the combination of the EPME and the subsequent prolonged interval of global warmth and environmental instability allowed new algal groups to expand and then become dominant in the post-Palaeozoic world.

6. Conclusions

The end-Permian mass extinction was a pivotal event that along with the subsequent climate perturbations of the Early Triassic brought about a fundamental shift in Earth's ecosystems. We provide new biomarker evidence (steranes and hopanes) for these shifts in the marine sections of the Sverdrup Basin, Arctic Canada and at Xiakou in South China that are integrated with other global records. Algal production, indicated by S/(S+H) ratios, had geographically diverse responses across the Permo-Triassic transition. Some sites, including the Sverdrup Basin, exhibited no immediate response to the EPME. The similarity of S/(S+H) ratios in the late Permian and the earliest Griesbachian indicates a rapid recovery of algal production following the EPME. The supposed post-EPME "collapse" in phytoplankton (e.g., Knoll et al., 2007a; Payne and van de Schootbrugge, 2007; Tappan, 1970; Twitchett, 2001) was likely temporally and spatially complex, reflecting the interplay of the biotic crisis with Early Triassic deoxygenation, nutrient limitation and high temperatures. Nonetheless, the EPME and Early Triassic appear to have been critical in the evolution of marine algal assemblages, as suggested by the increase in C_{28}/C_{29} ratios across the EPME at Meishan and by high values throughout most of the Griesbachian-Spathian interval in both the Sverdrup Basin and Chaohu sections. In particular, the correspondence between carbon cycle perturbations (CIEs in $\delta^{13}C_{org}$) and algal turnover inferred from C_{28}/C_{29}-ratios suggests a link between the Early Triassic carbon cycle and the eukaryotic algal revolution.

CRediT authorship contribution statement

Yizhou Huang: Investigation, Formal analysis, Data curation, Conceptualization, Writing – review & editing, Writing – original draft. **B. David A. Naafs:** Supervision, Writing – review & editing. **Richard D. Pancost:** Supervision, Data curation, Conceptualization, Writing – original draft. **Li Tian:** Writing – review & editing. **Stephen E. Grasby:** Writing – review & editing. **David P.G. Bond:** Writing – review & editing. **Paul B. Wignall:** Writing – review & editing. **Michael J. Benton:** Writing – review & editing.

Declaration of competing interest

The authors declare that they have no known competing financial interests or personal relationships that could have appeared to influence the work reported in this paper.

Acknowledgements

The research was supported by Natural Environment Research Council (contract no. NE/V003917/1) and funding from the European Research Council under the European Union's Seventh Framework Programme (FP/2007-2013) and European Research Council Grant Agreement number 340923 for funding GC–MS capabilities in Organic Geochemistry Unit, University of Bristol. The research was additionally supported by the Polar Continental Shelf Project for Arctic field work logistics. Y.H. acknowledges funding from the National Natural Science Foundation of China (grant no. 42293290). B.D.A.N. acknowledges funding through a Royal Society Tata University Research Fellowship. D. P.G.B. acknowledges funding from Natural Environment Research Council (grant no. NE/J01799X/1 and NE/V001639/1). L.T. acknowledges funding from the National Natural Science Foundation of China (grant no. 42272361).

Appendix A. Supplementary data

Supplementary data to this article can be found online at https://doi.org/10.1016/j.gloplacha.2025.105208.

Data availability

The authors confirm that all data necessary for supporting the scientific findings of this paper have been provided.

Biomarker data for Algal reorganization in post-crisis Early Triassic oceans revealed by biomarker evidence (Original data) (Figshare)

References

Algeo, T.J., Chen, Z.Q., Fraiser, M.L., Twitchett, R.J., 2011. Terrestrial-marine teleconnections in the collapse and rebuilding of early Triassic marine ecosystems. Palaeogeogr. Palaeoclimatol. Palaeoecol. 308 (1–2), 1–11. https://doi.org/10.1016/j.palaeo.2011.01.011.

Algeo, T.J., Henderson, C.M., Tong, J., Feng, Q., Yin, H., Tyson, R.V., 2013. Plankton and productivity during the Permian–Triassic boundary crisis: An analysis of organic carbon fluxes. Glob. Planet. Chang. 105, 52–67. https://doi.org/10.1016/j.gloplacha.2012.02.008.

Bachvaroff, T.R., Sanchez Puerta, M.V., Delwiche, C.F., 2005. Chlorophyll *c*-containing plastid relationships based on analyses of a multigene data set with all four chromalveolate lineages. Mol. Biol. Evol. 22 (9), 1772–1782. https://doi.org/10.1093/molbev/msi172.

Badger, M.R., von Caemmerer, S., Ruuska, S., Nakano, H., 2000. Electron flow to oxygen in higher plants and algae: rates and control of direct photoreduction (Mehler reaction) and rubisco oxygenase. Philos. Trans. R. Soc. Lond. B Biol. Sci. 355, 1433–1446. https://doi.org/10.1098/rstb.2000.0704.

Barton, D.H.R., Jarman, T.R., Watson, K.C., Widdowson, D.A., Boar, R.B., Damps, K., 1975. Investigations on the biosynthesis of steroids and terpenoids. Part XII. Biosynthesis of 3β-hydroxy-triterpenoids and -steroids from (3S)-2,3-epoxy-2,3-dihydrosqualene. J. Chem. Soc., Perkin Trans. 1 1 (12), 1134–1138. https://doi.org/10.1039/P19750001134.

Beauchamp, B., Grasby, S.E., 2012. Permian lysocline shoaling and ocean acidification along NW Pangea led to carbonate eradication and chert expansion. Palaeogeogr. Palaeoclimatol. Palaeoecol. 350–352, 73–90. https://doi.org/10.1016/j.palaeo.2012.06.014.

Beauchamp, B., Henderson, C.M., Grasby, S.E., Gates, L.T., Beatty, T.W., Utting, J., James, N.P., 2009. Late Permian sedimentation in the Sverdrup Basin, Canadian Arctic: the Lindstrom and Black Stripe Formations. Bull. Can. Petrol. Geol. 57 (2), 167–191. https://doi.org/10.2113/gscpgbull.57.2.167.

Belin, B.J., Busset, N., Giraud, E., Molinaro, A., Silipo, A., Newman, D.K., 2018. Hopanoid lipids: from membranes to plant–bacteria interactions. Nat. Rev. Microbiol. 16 (5), 304–315. https://doi.org/10.1038/nrmicro.2017.173.

Benton, M.J., Newell, A.J., 2014. Impacts of global warming on Permo-Triassic terrestrial ecosystems. Gondwana Res. 25 (4), 1308–1337. https://doi.org/10.1016/j.gr.2012.12.010.

Bobrovskiy, I., Poulton, S.W., Hope, J.M., Brocks, J.J., 2024. Impact of aerobic reworking of biomass on steroid and hopanoid biomarker parameters recording ecological conditions and thermal maturity. Geochim. Cosmochim. Acta 364, 114–128. https://doi.org/10.1016/j.gca.2023.11.024.

Bond, D.P.G., Grasby, S.E., 2017. On the causes of mass extinctions. Palaeogeogr. Palaeoclimatol. Palaeoecol. 478, 3–29. https://doi.org/10.1016/j.palaeo.2016.11.005.

Bond, D.P.G., Wignall, P.B., Grasby, S.E., 2020. The Capitanian (Guadalupian, Middle Permian) mass extinction in NW Pangea (Borup Fiord, Arctic Canada): a global crisis driven by volcanism and anoxia. Bull. Geol. Soc. Am. 132 (5–6), 931–942. https://doi.org/10.1130/B35281.1.

Büchel, C., 2020. Light harvesting complexes in chlorophyll *c*-containing algae. Biochim. Biophys. Acta (BBA) – Bioenerg. 1861 (4), 148027. https://doi.org/10.1016/j.bbabio.2019.05.003.

Burgess, S.D., Muirhead, J.D., Bowring, S.A., 2017. Initial pulse of Siberian Traps sills as the trigger of the end-Permian mass extinction. Nat. Commun. 8 (1), 1–4. https://doi.org/10.1038/s41467-017-00083-9.

Cao, C., Wang, W., Jin, Y., 2002. Carbon isotope excursions across the Permian-Triassic boundary in the Meishan section, Zhejiang Province, China. Chin. Sci. Bull. 47 (13), 1125–1129. https://doi.org/10.1360/02tb9252.

Cao, C., Love, G.D., Hays, L.E., Wang, W., Shen, S., Summons, R.E., 2009. Biogeochemical evidence for euxinic oceans and ecological disturbance presaging the end-Permian mass extinction event. Earth Planet. Sci. Lett. 281 (3–4), 188–201. https://doi.org/10.1016/j.epsl.2009.02.012.

Chen, Z., Benton, M.J., 2012. The timing and pattern of biotic recovery following the end-Permian mass extinction. Nat. Geosci. 5 (6), 375–383. https://doi.org/10.1038/ngeo1475.

Chen, Z., Tong, J., Fraiser, M.L., 2011. Trace fossil evidence for restoration of marine ecosystems following the end-Permian mass extinction in the lower Yangtze region, South China. Palaeogeogr. Palaeoclimatol. Palaeoecol. 299 (3–4), 449–474. https://doi.org/10.1016/j.palaeo.2010.11.023.

Chu, D., Corso, J.D., Shu, W., Song, H., Wignall, P.B., Grasby, S.E., van de Schootbrugge, B., Zong, K., Wu, Y., Tong, J., 2021. Metal-induced stress in survivor plants following the end-Permian collapse of land ecosystems. Geology 49 (6), 657–661. https://doi.org/10.1130/G48333.1.

Clarkson, M.O., Kasemann, S.A., Wood, R.A., Lenton, T.M., Daines, S.J., Richoz, S., Ohnemueller, F., Meixner, A., Poulton, S.W., Tipper, E.T., 2015. Ocean acidification and the Permo-Triassic mass extinction. Science 348 (6231), 229–232. https://doi.org/10.1126/science.aaa0193.

Collister, J.W., Summons, R.E., Lichtfouse, E., Hayes, J.M., 1992. An isotopic biogeochemical study of the Green River oil shale. Org. Geochem. 19 (1–3), 265–276. https://doi.org/10.1016/0146-6380(92)90042-V.

Cui, Y., Li, M., van Soelen, E.E., Peterse, F., Kürschner, W.M., 2021. Massive and rapid predominantly volcanic CO_2 emission during the end-Permian mass extinction. Proc. Natl. Acad. Sci. 118 (37), 1–11. https://doi.org/10.1073/pnas.2014701118.

Dal Corso, J., Mills, B.J.W., Chu, D., Newton, R.J., Mather, T.A., Shu, W., Wu, Y., Tong, J., Wignall, P.B., 2020. Permo–Triassic boundary carbon and mercury cycling linked to terrestrial ecosystem collapse. Nat. Commun. 11 (1), 1–9. https://doi.org/10.1038/s41467-020-16725-4.

Dal Corso, J., Song, H., Callegaro, S., Chu, D., Sun, Y., Hilton, J., Grasby, S.E., Joachimski, M.M., Wignall, P.B., 2022. Environmental crises at the Permian–Triassic mass extinction. Nat. Rev. Earth Environ. 3 (3), 197–214. https://doi.org/10.1038/s43017-021-00259-4.

de Clerck, O., Bogaert, K.A., Leliaert, F., 2012. Diversity and Evolution of Algae. In: Advances in Botanical Research, vol. 64. Academic Press Inc., pp. 55–86. https://doi.org/10.1016/B978-0-12-391499-6.00002-5

de Vargas, C., Aubry, M.-P., Probert, I., Young, J., 2007. Origin and Evolution of Coccolithophores: From Coastal Hunters to Oceanic Farmers. In: Evolution of Primary Producers in the Sea. Elsevier, pp. 251–285. https://doi.org/10.1016/B978-012370518-1/50013-8.

Dewing, K., Obermajer, M., 2011. Chapter 38: thermal maturity of the Sverdrup Basin, Arctic Canada and its bearing on hydrocarbon potential. Geol. Soc. Mem. 35, 567–580. https://doi.org/10.1144/M35.38.

Du, Y., Song, H.Y., Tong, J., Algeo, T.J., Li, Z., Song, H.J., Huang, J., 2021. Changes in productivity associated with algal-microbial shifts during the early Triassic recovery of marine ecosystems. Geol. Soc. Am. Bull. 133 (1–2), 362–378. https://doi.org/10.1130/B35510.1.

Du, Y., Song, H.Y., Grasby, S.E., Xing, T., Song, H.J., Tian, L., Chu, D., Wu, Y., Dal Corso, J., Algeo, T.J., Tong, J., 2023. Recovery from persistent nutrient-N limitation following the Permian–Triassic mass extinction. Earth Planet. Sci. Lett. 602, 117944. https://doi.org/10.1016/j.epsl.2022.117944.

Du, Y., Song, H.Y., Stüeken, E.E., Grasby, S.E., Song, H.J., Tian, L., Chu, D., Dal Corso, J., Li, Z., Tong, J., 2024. Large nitrogen cycle perturbations during the early Triassic hyperthermal. Geochim. Cosmochim. Acta 382, 13–25. https://doi.org/10.1016/j.gca.2024.08.009.

Embry, A., 1989. Correlation of Upper Palaeozoic and Mesozoic sequences between Svalbard, Canadian Arctic Archipelago, and northern Alaska. In: Correlation in Hydrocarbon Exploration, Vol. 57, Issue 2. Springer, Netherlands, pp. 89–98. https://doi.org/10.1007/978-94-009-1149-9_9.

Embry, A., Beauchamp, B., 2019. Sverdrup Basin. In: The Sedimentary Basins of the United States and Canada. Elsevier, pp. 559–592. https://doi.org/10.1016/B978-0-444-63895-3.00014-0.

Ezaki, Y., Liu, J., Adachi, N., 2003. Earliest Triassic microbialite micro- to megastructures in the Huaying Area of Sichuan Province, South China: Implications for the nature of oceanic conditions after the End-Permian Extinction. Palaios 18 (4–5), 388–402. https://doi.org/10.1669/0883-1351(2003)018<0388:ETMMTM>2.0.CO;2.

Falkowski, P.G., 1997. Evolution of the nitrogen cycle and its influence on the biological sequestration of CO_2 in the ocean. Nature 387 (6630), 272–275. https://doi.org/10.1038/387272a0.

Falkowski, P.G., Katz, M.E., Knoll, A.H., Quigg, A., Raven, J.A., Schofield, O., Taylor, F.J. R., 2004. The evolution of modern eukaryotic phytoplankton. Science 305 (5682), 354–360. https://doi.org/10.1126/science.1095964.

Fay, P., 1992. Oxygen relations of nitrogen fixation in cyanobacteria. Microbiol. Rev. 56 (2), 340–373. https://doi.org/10.1128/mr.56.2.340-373.1992.

Feng, Z., Bao, Z., Wu, S., Li, Y., Wang, G., 1997. Lithofacies Palaeogeography of The Early and Middle Triassic of South China. Chin. J. Geol. 32 (2), 212–220. (in Chinese with English abstract).

Feng, X., Chen, Z.-Q., Benton, M.J., Su, C., Bottjer, D.J., Cribb, A.T., Li, Z., Zhao, L., Zhu, G., Huang, Y., Guo, Z., 2022. Resilience of infaunal ecosystems during the early Triassic greenhouse Earth. Sci. Adv. 8 (26), 597. https://doi.org/10.1126/sciadv.abo0597.

Forkner, R.M., Dahl, J., Fildani, A., Barbanti, S.M., Yurchenko, I.A., Moldowan, J.M., 2021. Anatomy of an extinction revealed by molecular fossils spanning OAE2. Sci. Rep. 11 (1), 13621. https://doi.org/10.1038/s41598-021-92817-5.

Foster, W.J., Heindel, K., Richoz, S., Gliwa, J., Lehrmann, D.J., Baud, A., Kolar-Jurkovšek, T., Aljinović, D., Jurkovšek, B., Korn, D., Martindale, R.C., Peckmann, J., 2020. Suppressed competitive exclusion enabled the proliferation of Permian/Triassic boundary microbialites. Depositional Rec. 6 (1), 62–74. https://doi.org/10.1002/dep2.97.

Fraiser, M.L., Bottjer, D.J., 2007. Elevated atmospheric CO_2 and the delayed biotic recovery from the end-Permian mass extinction. Palaeogeogr. Palaeoclimatol. Palaeoecol. 252 (1–2), 164–175. https://doi.org/10.1016/j.palaeo.2006.11.041.

Galfetti, T., Bucher, H., Martini, R., Hochuli, P.A., Weissert, H., Crasquin-Soleau, S., Brayard, A., Goudemand, N., Brühwiler, T., Guodun, K., 2008. Evolution of early Triassic outer platform paleoenvironments in the Nanpanjiang Basin (South China) and their significance for the biotic recovery. Sediment. Geol. 204 (1–2), 36–60. https://doi.org/10.1016/j.sedgeo.2007.12.008.

Galloway, B.J., Dewing, K., Beauchamp, B., 2018. Upper Paleozoic hydrocarbon systems in the Sverdrup Basin, Canadian Arctic Islands. Mar. Pet. Geol. 92 (December 2017), 809–821. https://doi.org/10.1016/j.marpetgeo.2017.12.013.

Gao, Q., Zhang, N., Xia, W., Feng, Q., Chen, Z.Q., Zheng, J., Griffin, W.L., O'Reilly, S.Y., Pearson, N.J., Wang, G., Wu, S., Zhong, W., Sun, X., 2013. Origin of volcanic ash beds across the permian-triassic boundary, daxiakou, South China: Petrology and U-Pb age, trace elements and Hf-isotope composition of zircon. Chem. Geol. 360–361, 41–53. https://doi.org/10.1016/j.chemgeo.2013.09.020.

Gardin, S., Krystyn, L., Richoz, S., Bartolini, A., Galbrun, B., 2012. Where and when the earliest coccolithophores? Lethaia 45 (4), 507–523. https://doi.org/10.1111/j.1502-3931.2012.00311.x.

Ge, X., Chen, D., Zhang, G., Huang, T., Liu, M., El-Shafeiy, M., 2022. Marine redox evolution and organic accumulation in an intrashelf basin, NE Sichuan Basin during the late Permian. Mar. Pet. Geol. 140, 105633. https://doi.org/10.1016/j.marpetgeo.2022.105633.

Georgiev, S.V., Horner, T.J., Stein, H.J., Hannah, J.L., Bingen, B., Rehkämper, M., 2015. Cadmium-isotopic evidence for increasing primary productivity during the late Permian anoxic event. Earth Planet. Sci. Lett. 410, 84–96. https://doi.org/10.1016/j.epsl.2014.11.010.

Goss, R., Jakob, T., 2010. Regulation and function of xanthophyll cycle-dependent photoprotection in algae. Photosynth. Res. 106 (1–2), 103–122. https://doi.org/10.1007/s11120-010-9536-x.

Grantham, P.J., Wakefield, L.L., 1988. Variations in the sterane carbon number distributions of marine source rock derived crude oils through geological time. Org. Geochem. 12 (1), 61–73. https://doi.org/10.1016/0146-6380(88)90115-5.

Grasby, S.E., Beauchamp, B., 2008. Intrabasin variability of the carbon-isotope record across the Permian-Triassic transition, Sverdrup Basin, Arctic Canada. Chem. Geol. 253 (3–4), 141–150. https://doi.org/10.1016/j.chemgeo.2008.05.005.

Grasby, S.E., Beauchamp, B., 2009. Latest Permian to early Triassic basin-to-shelf anoxia in the Sverdrup Basin, Arctic Canada. Chem. Geol. 264 (1–4), 232–246. https://doi.org/10.1016/j.chemgeo.2009.03.009.

Grasby, S.E., Beauchamp, B., Embry, A., Sanei, H., 2013. Recurrent early Triassic Ocean anoxia. Geology 41 (2), 175–178. https://doi.org/10.1130/G33599.1.

Grasby, S.E., Beauchamp, B., Knies, J., 2016. Early Triassic productivity crises delayed recovery from world's worst mass extinction. Geology 44 (9), 779–782. https://doi.org/10.1130/G38141.1.

Grasby, S.E., Bond, D.P.G., Wignall, P.B., Beauchamp, B., 2026. The late Permian through Middle Triassic environmental crises in the Boreal Realm – Records of the Griesbachian, Dienerian, Smithian, and Spathian type sections in Arctic Canada. Palaeogeogr. Palaeoclimatol. Palaeoecol. 682, 113453. https://doi.org/10.1016/j.palaeo.2025.113453.

Grasby, S.E., Knies, J., Beauchamp, B., Bond, D.P.G., Wignall, P., Sun, Y., 2020. Global warming leads to early Triassic nutrient stress across northern Pangea. Geol. Soc. Am. Bull. 132 (5–6), 943–954. https://doi.org/10.1130/B32036.1.

Grasby, S.E., Ardakani, O.H., Liu, X., Bond, D.P.G., Wignall, P.B., Strachan, L.J., 2023. Marine snowstorm during the Permian−Triassic mass extinction. Geology 52 (2), 120–124. https://doi.org/10.1130/G51497.1.

Grice, K., 2005. Photic Zone Euxinia During the Permian-Triassic Superanoxic Event. Science 307 (5710), 706–709. https://doi.org/10.1126/science.1104323.

Grisdale, C.J., Archibald, J.M., 2017. Secondary and Tertiary Endosymbiosis☆. In: Reference Module in Life Sciences. Elsevier, pp. 201–210. https://doi.org/10.1016/B978-0-12-809633-8.13107-3.

Haubrich, B.A., Collins, E.K., Howard, A.L., Wang, Q., Snell, W.J., Miller, M.B., Thomas, C.D., Pleasant, S.K., Nes, W.D., 2015. Characterization, mutagenesis and mechanistic analysis of an ancient algal sterol C24-methyltransferase: Implications for understanding sterol evolution in the green lineage. Phytochemistry 113, 64–72. https://doi.org/10.1016/j.phytochem.2014.07.019.

Hays, L.E., Grice, K., Foster, C.B., Summons, R.E., 2012. Biomarker and isotopic trends in a Permian–Triassic sedimentary section at Kap Stosch, Greenland. Org. Geochem. 43, 67–82. https://doi.org/10.1016/J.ORGGEOCHEM.2011.10.010.

Heindel, K., Foster, W.J., Richoz, S., Birgel, D., Roden, V.J., Baud, A., Brandner, R., Krystyn, L., Mohtat, T., Koşun, E., Twitchett, R.J., Reitner, J., Peckmann, J., 2018. The formation of microbial-metazoan bioherms and biostromes following the latest Permian mass extinction. Gondwana Res. 61, 187–202. https://doi.org/10.1016/j.gr.2018.05.007.

Higgins, M.B., Robinson, R.S., Husson, J.M., Carter, S.J., Pearson, A., 2012. Dominant eukaryotic export production during ocean anoxic events reflects the importance of recycled NH_4^+. Proc. Natl. Acad. Sci. 109 (7), 2269–2274. https://doi.org/10.1073/pnas.1104313109.

Hoshino, Y., Gaucher, E.A., 2021. Evolution of bacterial steroid biosynthesis and its impact on eukaryogenesis. Proc. Natl. Acad. Sci. 118 (25), 1–9. https://doi.org/10.1073/pnas.2101276118.

Huang, W.-Y., Meinschein, W.G., 1979. Sterols as ecological indicators. Geochim. Cosmochim. Acta 43 (5), 739–745. https://doi.org/10.1016/0016-7037(79)90257-6.

Huang, J., Luo, G., Bai, X., Tang, X., 2007. Organic fraction of the total carbon burial flux deduced from carbon isotopes across the Permo-Triassic boundary at Meishan, Zhejiang Province, China. Front. Earth Sci. China 1 (4), 425–430. https://doi.org/10.1007/s11707-007-0052-z.

Idle, D.R., Wisman, P., 1971. Sterols of crustacea. Int. J. Biochem. 2 (7), 91–98. https://doi.org/10.1016/0020-711X(71)90046-2.

Isaksen, G.H., 1995. Organic Geochemistry of Paleodepositional Environments with a Predominance of Terrigenous Higher-Plant Organic Matter. In: Paleogeography, Paleoclimate, and Source Rocks. American Association of Petroleum Geologists. https://doi.org/10.1306/St40595C4.

Jia, C., Huang, J., Kershaw, S., Luo, G., Farabegoli, E., Perri, M.C., Chen, L., Bai, X., Xie, S., 2012. Microbial response to limited nutrients in shallow water immediately after the end-Permian mass extinction. Geobiology 10 (1), 60–71. https://doi.org/10.1111/j.1472-4669.2011.00310.x.

Joachimski, M.M., Alekseev, A.S., Grigoryan, A., Gatovsky, Yu.A., 2020. Siberian Trap volcanism, global warming and the Permian-Triassic mass extinction: New insights from Armenian Permian-Triassic sections. Geol. Soc. Am. Bull. 132 (1–2), 427–443. https://doi.org/10.1130/B35108.1.

Joachimski, M.M., Müller, J., Gallagher, T.M., Mathes, G., Chu, D.L., Mouraviev, F., Silantiev, V., Sun, Y.D., Tong, J.N., 2022. Five million years of high atmospheric CO_2 in the aftermath of the Permian-Triassic mass extinction. Geology 50 (6), 650–654. https://doi.org/10.1130/G49714.1.

Khan, A.K., Kausar, H., Jaferi, S.S., Drouet, S., Hano, C., Abbasi, B.H., Anjum, S., 2020. An insight into the algal evolution and genomics. Biomolecules 10 (11), 1524. https://doi.org/10.3390/biom10111524.

Knies, J., Grasby, S.E., Beauchamp, B., Schubert, C.J., 2013. Water mass denitrification during the latest Permian extinction in the Sverdrup Basin, Arctic Canada. Geology 41 (2), 167–170. https://doi.org/10.1130/G33816.1.

Knies, J., Schönenberger, J., Zwingmann, H., van der Lelij, R., Smelror, M., Vullum, P.E., Brönner, M., Vogt, C., Fredin, O., Müller, A., Grasby, S.E., Beauchamp, B., Viola, G., 2022. Continental weathering and recovery from ocean nutrient stress during the early Triassic Biotic Crisis. Commun. Earth Environ. 3 (1), 1–12. https://doi.org/10.1038/s43247-022-00480-z.

Knoll, A.H., Bambach, R.K., Payne, J.L., Pruss, S., Fischer, W.W., 2007a. Paleophysiology and end-Permian mass extinction. Earth Planet. Sci. Lett. 256 (3–4), 295–313. https://doi.org/10.1016/j.epsl.2007.02.018.

Knoll, A.H., Summons, R.E., Waldbauer, J.R., Zumberge, J.E., 2007b. The Geological Succession of primary producers in the Oceans. In: Evolution of Primary Producers in the Sea. Elsevier, pp. 133–163. https://doi.org/10.1016/B978-012370518-1/50009-6.

Kodner, R.B., Pearson, A., Summons, R.E., Knoll, A.H., 2008. Sterols in red and green algae: quantification, phylogeny, and relevance for the interpretation of geologic steranes. Geobiology 6 (4), 411–420. https://doi.org/10.1111/j.1472-4669.2008.00167.x.

Kump, L.R., 2018. Prolonged Late Permian–Early Triassic hyperthermal: Failure of climate regulation? Philos. Trans. R. Soc. A Math. Phys. Eng. Sci. 376 (2130), 1–9. https://doi.org/10.1098/rsta.2017.0078.

Lau, K.V., Maher, K., Altiner, D., Kelley, B.M., Kump, L.R., Lehrmann, D.J., Silva-Tamayo, J.C., Weaver, K.L., Yu, M., Payne, J.L., 2016. Marine anoxia and delayed Earth system recovery after the end-Permian extinction. Proc. Natl. Acad. Sci. 113 (9), 2360–2365. https://doi.org/10.1073/pnas.1515080113.

Lei, L.D., Shen, J., Li, C., Algeo, T.J., Chen, Z.Q., Feng, Q.L., Cheng, M., Jin, C.S., Huang, J.H., 2017. Controls on regional marine redox evolution during Permian-Triassic transition in South China. Palaeogeogr. Palaeoclimatol. Palaeoecol. 486, 17–32. https://doi.org/10.1016/j.palaeo.2017.02.010.

Liao, Z., Hu, W., Cao, J., Wang, X., Fu, X., 2020. Oceanic anoxia through the late Permian Changhsingian Stage in the lower Yangtze region, South China: evidence from sulfur isotopes and trace elements. Chem. Geol. 532, 1–15. https://doi.org/10.1016/j.chemgeo.2019.119371.

Liu, S.-A., Wu, H., Shen, S., Jiang, G., Zhang, S., Lv, Y., Zhang, H., Li, S., 2017. Zinc isotope evidence for intensive magmatism immediately before the end-Permian mass extinction. Geology 45 (4), 343–346. https://doi.org/10.1130/G38644.1.

Liu, W., Yao, J., Tong, J., Qiao, Y., Chen, Y., 2019. Organic matter accumulation on the Dalong Formation (Upper Permian) in western Hubei, South China: Constraints from multiple geochemical proxies and pyrite morphology. Palaeogeogr. Palaeoclimatol. Palaeoecol. 514, 677–689. https://doi.org/10.1016/j.palaeo.2018.11.015.

Liu, F., Peng, H., Marshall, J.E.A., Lomax, B.H., Bomfleur, B., Kent, M.S., Fraser, W.T., Jardine, P.E., 2023. Dying in the Sun: Direct evidence for elevated UV-B radiation at the end-Permian mass extinction. Sci. Adv. 9 (1), 1–11. https://doi.org/10.1126/sciadv.abo6102.

Luo, G., Huang, J., Xie, S., Wignall, P.B., Tang, X., Huang, X., Yin, H., 2010. Relationships between carbon isotope evolution and variation of microbes during the Permian-Triassic transition at Meishan Section, South China. Int. J. Earth Sci. 99 (4), 775–784. https://doi.org/10.1007/s00531-009-0421-9.

Luo, G., Wang, Y., Algeo, T.J., Kump, L.R., Bai, X., Yang, H., Yao, L., Xie, S., 2011. Enhanced nitrogen fixation in the immediate aftermath of the latest Permian marine mass extinction. Geology 39 (7), 647–650. https://doi.org/10.1130/G32024.1.

Luo, G., Wang, Y., Grice, K., Kershaw, S., Algeo, T.J., Ruan, X., Yang, H., Jia, C., Xie, S., 2013. Microbial-algal community changes during the latest Permian ecological crisis: evidence from lipid biomarkers at Cili, South China. Glob. Planet. Chang. 105, 36–51. https://doi.org/10.1016/j.gloplacha.2012.11.015.

Mackenzie, A.S., 1984. Applications of Biological Markers in Petroleum Geochemistry. In: Brooks, J., Welte, D. (Eds.), Advances in Petroleum Geochemistry, vol. 1. Academic Press, pp. 115–214.

Mackenzie, A.S., Patience, R.L., Maxwell, J.R., Vandenbroucke, M., Durand, B., 1980. Molecular parameters of maturation in the Toarcian shales, Paris Basin, France—I. Changes in the configurations of acyclic isoprenoid alkanes, steranes and triterpanes. Geochim. Cosmochim. Acta 44 (11), 1709–1721. https://doi.org/10.1016/0016-7037(80)90222-7.

Mays, C., McLoughlin, S., Frank, T.D., Fielding, C.R., Slater, S.M., Vajda, V., 2021. Lethal microbial blooms delayed freshwater ecosystem recovery following the end-Permian extinction. Nat. Commun. 12 (1). https://doi.org/10.1038/s41467-021-25711-3.

Meyer, K.M., Yu, M., Jost, A.B., Kelley, B.M., Payne, J.L., 2011. $\delta^{13}C$ evidence that high primary productivity delayed recovery from end-Permian mass extinction. Earth Planet. Sci. Lett. 302 (3–4), 378–384. https://doi.org/10.1016/j.epsl.2010.12.033.

Moldowan, J.M., Seifert, W.K., Gallegos, E.J., 1985. Relationship between petroleum composition and depositional environment of petroleum source rocks. Am. Assoc. Pet. Geol. Bull. 69 (8), 1255–1268. https://doi.org/10.1306/AD462BC8-16F7-11D7-8645000102C1865D.

Mouradian, M., Panetta, R.J., De Vernal, A., Gélinas, Y., 2007. Dinosterols or dinocysts to estimate dinoflagellate contributions to marine sedimentary organic matter? Limnol. Oceanogr. 52 (6), 2569–2581. https://doi.org/10.4319/lo.2007.52.6.2569.

Naafs, B.D.A., Monteiro, F.M., Pearson, A., Higgins, M.B., Pancost, R.D., Ridgwell, A., 2019. Fundamentally different global marine nitrogen cycling in response to severe ocean deoxygenation. Proc. Natl. Acad. Sci. 116 (50), 24979–24984. https://doi.org/10.1073/pnas.1905553116.

Naafs, B.D.A., Bianchini, G., Monteiro, F.M., Sánchez-Baracaldo, P., 2022. The occurrence of 2-methylhopanoids in modern bacteria and the geological record. Geobiology 20 (1), 41–59. https://doi.org/10.1111/gbi.12465.

Nakov, T., Beaulieu, J.M., Alverson, A.J., 2018. Accelerated diversification is related to life history and locomotion in a hyperdiverse lineage of microbial eukaryotes (Diatoms, *Bacillariophyta*). New Phytol. 219 (1), 462–473. https://doi.org/10.1111/nph.15137.

Nalley, J.O., O'Donnell, D.R., Litchman, E., 2018. Temperature effects on growth rates and fatty acid content in freshwater algae and cyanobacteria. Algal Res. 35, 500–507. https://doi.org/10.1016/j.algal.2018.09.018.

Nes, W.R., 1977. The Biochemistry of Plant Sterols, pp. 233–324. https://doi.org/10.1016/B978-0-12-024915-2.50010-4.

Nes, W.D., 2000. Sterol methyl transferase: Enzymology and inhibition. Biochim. Biophys. Acta (BBA) - Mol. Cell Biol. Lipids 1529 (1–3), 63–88. https://doi.org/10.1016/S1388-1981(00)00138-4.

Nes, W.D., 2003. Enzyme mechanisms for sterol *C*-methylations. Phytochemistry 64 (1), 75–95. https://doi.org/10.1016/S0031-9422(03)00349-2.

Nes, W.D., 2011. Biosynthesis of cholesterol and other sterols. Chem. Rev. 111 (10), 6423–6451. https://doi.org/10.1021/cr200021m.

Nowicka, B., 2022. Heavy metal–induced stress in eukaryotic algae—mechanisms of heavy metal toxicity and tolerance with particular emphasis on oxidative stress in exposed cells and the role of antioxidant response. Environ. Sci. Pollut. Res. 29 (12), 16860–196911. https://doi.org/10.1007/s11356-021-18419-w.

Ourisson, G., Albrecht, P., Rohmer, M., 1979. The hopanoids: palaeo-chemistry and biochemistry of a group of natural products. Pure Appl. Chem. 51 (4), 709–729. https://doi.org/10.1351/pac197951040709.

Ourisson, G., de Neurochimie, C., Pascal, B., Rohmer, M., Nationale, E., de Chimie, S., Werner, A.I.I.B., Tiibingen, U., der Morgenstelle, A., 1987. Prokaryotic hopanoids and other polyterpenoid sterol surrogates. Ann. Rev. Microbiol. 41 (1), 301–333. https://doi.org/10.1146/annurev.mi.41.100187.001505.

Paerl, H.W., Otten, T.G., 2013. Harmful cyanobacterial blooms: Causes, consequences, and controls. Microb. Ecol. 65 (4), 995–1010. https://doi.org/10.1007/s00248-012-0159-y.

Payne, J.L., van de Schootbrugge, B., 2007. Life in Triassic Oceans: Links between Planktonic and Benthic Recovery and Radiation. In: Evolution of Primary Producers in the Sea. Elsevier, pp. 165–189. https://doi.org/10.1016/B978-012370518-1/50010-2.

Payne, J.L., Turchyn, A.V., Paytan, A., DePaolo, D.J., Lehrmann, D.J., Yu, M., Wei, J., 2010. Calcium isotope constraints on the end-Permian mass extinction. Proc. Natl. Acad. Sci. 107 (19), 8543–8548. https://doi.org/10.1073/pnas.0914065107.

Pearson, A., Budin, M., Brocks, J.J., 2003. Phylogenetic and biochemical evidence for sterol synthesis in the bacterium *Gemmata obscuriglobus*. Proc. Natl. Acad. Sci. 100 (26), 15352–15357. https://doi.org/10.1073/pnas.2536559100.

Peters, K.E., Moldowan, J.M., 1991. Effects of source, thermal maturity, and biodegradation on the distribution and isomerization of homohopanes in petroleum. Org. Geochem. 17 (1), 47–61. https://doi.org/10.1016/0146-6380(91)90039-M.

Peters, K.E., Walters, C.C., Moldowan, J.M., 2004. The Biomarker Guide (Second). Cambridge University Press. https://doi.org/10.1017/CBO9781107326040.

Peters, K.E., Moldowan, J.M., LaCroce, M.V., Kubicki, J.D., 2014. Stereochemistry, elution order and molecular modeling of four diaergostanes in petroleum. Org. Geochem. 76, 1–8. https://doi.org/10.1016/j.orggeochem.2014.07.008.

Pirnik, M.P., Atlas, R.M., Bartha, R., 1974. Hydrocarbon Metabolism by *Brevibacterium erythrogenes*: Normal and Branched Alkanes. J. Bacteriol. 119 (3), 868–878. https://doi.org/10.1128/jb.119.3.868-878.1974.

Qiu, Z., Song, H.J., Hu, C., Wignall, P.B., Song, H.Y., 2019. Carbonate thermoluminescence and its implication for marine productivity change during the Permian-Triassic transition. Palaeogeogr. Palaeoclimatol. Palaeoecol. 526, 72–79. https://doi.org/10.1016/j.palaeo.2019.04.021.

Rampen, S.W., Abbas, B.A., Schouten, S., Damsté, J.S.S., 2010. A comprehensive study of sterols in marine diatoms (*Bacillariophyta*): Implications for their use as tracers for diatom productivity. Limnol. Oceanogr. 55 (1), 91–105. https://doi.org/10.4319/lo.2010.55.1.0091.

Retallack, G.J., Conde, G.D., 2020. Deep time perspective on rising atmospheric CO_2. Glob. Planet. Chang. 189, 103177. https://doi.org/10.1016/j.gloplacha.2020.103177.

Riolo, J., Hussler, G., Albrecht, P., Connan, J., 1986. Distribution of aromatic steroids in geological samples: their evaluation as geochemical parameters. Org. Geochem. 10 (4–6), 981–990. https://doi.org/10.1016/S0146-6380(86)80036-5.

Rohmer, M., Bouvier-Nave, P., Ourisson, G., 1984. Distribution of hopanoid triterpenes in prokaryotes. Microbiology 130 (5), 1137–1150. https://doi.org/10.1099/00221287-130-5-1137.

Rubinstein, I., Sieskind, O., Albrecht, P., 1975. Rearranged sterenes in a shale: Occurrence and simulated formation. J. Chem. Soc. Perkin Trans. 1 (19), 1833. https://doi.org/10.1039/p19750001833.

Sáenz, J.P., Sezgin, E., Schwille, P., Simons, K., 2012. Functional convergence of hopanoids and sterols in membrane ordering. Proc. Natl. Acad. Sci. 109 (35), 14236–14240. https://doi.org/10.1073/pnas.1212141109.

Sáenz, J.P., Grosser, D., Bradley, A.S., Lagny, T.J., Lavrynenko, O., Broda, M., Simons, K., 2015. Hopanoids as functional analogues of cholesterol in bacterial membranes. Proc. Natl. Acad. Sci. 112 (38), 11971–11976. https://doi.org/10.1073/pnas.1515607112.

Sahney, S., Benton, M.J., 2008. Recovery from the most profound mass extinction of all time. Proc. R. Soc. B Biol. Sci. 275 (1636), 759–765. https://doi.org/10.1098/rspb.2007.1370.

Saito, R., Oba, M., Kaiho, K., Schaeffer, P., Adam, P., Takahashi, S., Watanabe Nara, F., Chen, Z.Q., Tong, J., Tsuchiya, N., 2014. Extreme euxinia just prior to the Middle Triassic biotic recovery from the latest Permian mass extinction. Org. Geochem. 73, 113–122. https://doi.org/10.1016/j.orggeochem.2014.05.007.

Saito, R., Kaiho, K., Oba, M., Tong, J., Chen, Z.Q., Takahashi, S., Chen, J., Tian, L., Biswas, R.K., 2016. Secular changes in environmental stresses and eukaryotes during the early Triassic to the early Middle Triassic. Palaeogeogr. Palaeoclimatol. Palaeoecol. 451, 35–45. https://doi.org/10.1016/j.palaeo.2016.03.006.

Saitoh, M., Ueno, Y., Nishizawa, M., Isozaki, Y., Takai, K., Yao, J., Ji, Z., 2014. Nitrogen isotope chemostratigraphy across the Permian–Triassic boundary at Chaotian, Sichuan, South China. J. Asian Earth Sci. 93, 113–128. https://doi.org/10.1016/j.jseaes.2014.06.026.

Sanson-Barrera, A., Hochuli, P.A., Bucher, H., Schneebeli-Hermann, E., Weissert, H., Adatte, T., Bernasconi, S.M., 2015. Late Permian-earliest Triassic high-resolution organic carbon isotope and palynofacies records from Kap Stosch (East Greenland). Glob. Planet. Chang. 133, 149–166. https://doi.org/10.1016/j.gloplacha.2015.08.006.

Schneebeli-Hermann, E., Hochuli, P.A., Bucher, H., 2017. Palynofloral associations before and after the Permian–Triassic mass extinction, Kap Stosch, East Greenland. Glob. Planet. Chang. 155, 178–195. https://doi.org/10.1016/j.gloplacha.2017.06.009.

Schobben, M., Stebbins, A., Ghaderi, A., Strauss, H., Korn, D., Korte, C., 2015. Flourishing Ocean drives the end-Permian marine mass extinction. Proc. Natl. Acad. Sci. 112 (33), 10298–10303. https://doi.org/10.1073/pnas.1503755112.

Schobben, M., Foster, W.J., Sleveland, A.R.N., Zuchuat, V., Svensen, H.H., Planke, S., Bond, D.P.G., Marcelis, F., Newton, R.J., Wignall, P.B., Poulton, S.W., 2020. A nutrient control on marine anoxia during the end-Permian mass extinction. Nat. Geosci. 13 (9), 640–646. https://doi.org/10.1038/s41561-020-0622-1.

Schoepfer, S.D., Henderson, C.M., Garrison, G.H., Foriel, J., Ward, P.D., Selby, D., Hower, J.C., Algeo, T.J., Shen, Y., 2013. Termination of a continent-margin upwelling system at the Permian–Triassic boundary (Opal Creek, Alberta, Canada). Glob. Planet. Chang. 105, 21–35. https://doi.org/10.1016/j.gloplacha.2012.07.005.

Schwark, L., Empt, P., 2006. Sterane biomarkers as indicators of palaeozoic algal evolution and extinction events. Palaeogeogr. Palaeoclimatol. Palaeoecol. 240 (1–2), 225–236. https://doi.org/10.1016/j.palaeo.2006.03.050.

Scotese, C.R., 2014. Atlas of Jurassic Paleogeographic Maps. In: PALEOMAP Atlas for ArcGIS, 3, The Jurassic and Triassic, Maps 32-42, Mollweide Projection. PALEOMAP Project, Evanston, IL.

Seifert, W.K., Moldowan, J.M., 1979. The effect of biodegradation on steranes and terpanes in crude oils. Geochim. Cosmochim. Acta 43 (1), 111–126. https://doi.org/10.1016/0016-7037(79)90051-6.

Seifert, W.K., Moldowan, J.M., 1980. The effect of thermal stress on source-rock quality as measured by hopane stereochemistry. Phys. Chem. Earth 12 (C), 229–237. https://doi.org/10.1016/0079-1946(79)90107-1.

Senowbari-Daryan, B., Link, M., Isintek, I., 2006. Calcareous algae from the Triassic (Anisian reef boulders and Norian reef limestones) of Karaburun, western Turkey. Facies 52 (1), 129–148. https://doi.org/10.1007/s10347-005-0025-1.

Sepúlveda, J., Wendler, J.E., Summons, R.E., Hinrichs, K.-U., 2009. Rapid resurgence of marine productivity after the Cretaceous-Paleogene Mass Extinction. Science 326 (5949), 129–132. https://doi.org/10.1126/science.1176233.

Shen, S., Crowley, J.L., Wang, Y., Bowring, S.A., Erwin, D.H., Sadler, P.M., Cao, C., Rothman, D.H., Henderson, C.M., Ramezani, J., Zhang, H., Shen, Y., Wang, X., Wang, W., Mu, L., Li, W., Tang, Y., Liu, X., Liu, L., Zeng, Y., Jiang, Y., Jin, Y., 2011. Calibrating the End-Permian Mass Extinction. Science 334 (6061), 1367–1372. https://doi.org/10.1126/science.1213454.

Shen, J., Zhou, L., Feng, Q.L., Zhang, M.H., Lei, Y., Zhang, N., Yu, J.X., Gu, S.Z., 2014. Paleo-productivity evolution across the Permian-Triassic boundary and quantitative calculation of primary productivity of black rock series from the Dalong Formation, South China. Sci. China Earth Sci. 57 (7), 1583–1594. https://doi.org/10.1007/s11430-013-4780-5.

Shen, J., Schoepfer, S.D., Feng, Q., Zhou, L., Yu, J., Song, H., Wei, H., Algeo, T.J., 2015. Marine productivity changes during the end-Permian crisis and early Triassic recovery. Earth Sci. Rev. 149, 136–162. https://doi.org/10.1016/j.earscirev.2014.11.002.

Shen, J., Feng, Q., Algeo, T.J., Li, C., Planavsky, N.J., Zhou, L., Zhang, M., 2016. Two pulses of oceanic environmental disturbance during the Permian-Triassic boundary crisis. Earth Planet. Sci. Lett. 443, 139–152. https://doi.org/10.1016/j.epsl.2016.03.030.

Simonin, P., Jürgens, U.J., Rohmer, M., 1992. 35-O-β-Amino-deoxyglucopyranosyl bacteriohopanetetrol, a novel triterpenoid of the hopane series from the cyanobacterium *synechocystis sp.* PCC 6714. Tetrahedron Lett. 33 (25), 3629–3632. https://doi.org/10.1016/S0040-4039(00)92520-6.

Simonin, P., Jürgens, U.J., Rohmer, M., 1996. Bacterial triterpenoids of the hopane series from the prochlorophyte *Prochlorothrix hollandica* and their intracellular localization. Eur. J. Biochem. 241 (3), 865–871. https://doi.org/10.1111/j.1432-1033.1996.00865.x.

Slater, S.M., Twitchett, R.J., Danise, S., Vajda, V., 2019. Substantial vegetation response to early Jurassic global warming with impacts on oceanic anoxia. Nat. Geosci. 12 (6), 462–467. https://doi.org/10.1038/s41561-019-0349-z.

Song, H.J., Wignall, P.B., Chen, Z.-Q., Tong, J., Bond, D.P.G., Lai, X., Zhao, X., Jiang, H., Yan, C., Niu, Z., Chen, J., Yang, H., Wang, Y., 2011. Recovery tempo and pattern of marine ecosystems after the end-Permian mass extinction. Geology 39 (8), 739–742. https://doi.org/10.1130/G32191.1.

Song, H.Y., Du, Y., Algeo, T.J., Tong, J., Owens, J.D., Song, H.J., Tian, L., Qiu, H., Zhu, Y., Lyons, T.W., 2019. Cooling-driven oceanic anoxia across the Smithian/Spathian boundary (mid-early Triassic). Earth Sci. Rev. 195 (January), 133–146. https://doi.org/10.1016/j.earscirev.2019.01.009.

Song, H.J., Song, H.Y., Tong, J., Gordon, G.W., Wignall, P.B., Tian, L., Zheng, W., Algeo, T.J., Liang, L., Bai, R., Wu, K., Anbar, A.D., 2021. Conodont calcium isotopic evidence for multiple shelf acidification events during the early Triassic. Chem. Geol. 562, 120038. https://doi.org/10.1016/j.chemgeo.2020.120038.

Sosa-Montes de Oca, C., Taylor, K.W.R., Hollis, C., Huang, Y., Pancost, R.D., 2023. Variation in organic matter across the Cretaceous-Paleogene Boundary in New Zealand supports the “living ocean” model of biotic recovery. Glob. Planet. Chang. 220, 104025. https://doi.org/10.1016/j.gloplacha.2022.104025.

Stanley, S.M., 2009. Evidence from ammonoids and conodonts for multiple early Triassic mass extinctions. Proc. Natl. Acad. Sci. 106 (36), 15264–15267. https://doi.org/10.1073/pnas.0907992106.

Summons, R.E., Thomas, J., Maxwell, J.R., Boreham, C.J., 1992. Secular and environmental constraints on the occurrence of dinosterane in sediments. Geochim. Cosmochim. Acta 56 (6), 2437–2444. https://doi.org/10.1016/0016-7037(92)90200-3.

Summons, R.E., Jahnke, L.L., Hope, J.M., Logan, G.A., 1999. 2-Methylhopanoids as biomarkers for cyanobacterial oxygenic photosynthesis. Nature 400 (6744), 554–557. https://doi.org/10.1038/23005.

Sun, Y., Joachimski, M.M., Wignall, P.B., Yan, C., Chen, Y., Jiang, H., Wang, L., Lai, X., 2012. Lethally hot temperatures during the early Triassic greenhouse. Science 338 (6105), 366–370. https://doi.org/10.1126/science.1224126.

Sun, Y., Zulla, M.J., Joachimski, M.M., Bond, D.P.G., Wignall, P.B., Zhang, Z.T., Zhang, M.H., 2019. Ammonium ocean following the end-Permian mass extinction. Earth Planet. Sci. Lett. 518, 211–222. https://doi.org/10.1016/j.epsl.2019.04.036.

Suzuki, N., Ishida, K., Shinomiya, Y., Ishiga, H., 1998. High productivity in the earliest Triassic Ocean: Black shales, Southwest Japan. Palaeogeogr. Palaeoclimatol. Palaeoecol. 141 (1–2), 53–65. https://doi.org/10.1016/S0031-0182(98)00009-1.

Takahashi, S., Yamakita, S., Suzuki, N., Kaiho, K., Ehiro, M., 2009. High organic carbon content and a decrease in radiolarians at the end of the Permian in a newly discovered continuous pelagic section: a coincidence? Palaeogeogr. Palaeoclimatol. Palaeoecol. 271 (1–2), 1–12. https://doi.org/10.1016/j.palaeo.2008.08.016.

Tappan, H., 1970. Phytoplankton abundance and late Paleozoic extinctions: a reply. Palaeogeogr. Palaeoclimatol. Palaeoecol. 8 (1), 56–66.

Tong, J., Zhao, L., 2011. Lower Triassic and Induan-Olenekian Boundary in Chaohu, Anhui Province, South China. Acta Geol. Sin. (Engl. Ed.) 85 (2), 399–407. https://doi.org/10.1111/j.1755-6724.2011.00408.x.

Trotter, J.A., Williams, I.S., Nicora, A., Mazza, M., Rigo, M., 2015. Long-term cycles of Triassic climate change: a new $\delta^{18}O$ record from conodont apatite. Earth Planet. Sci. Lett. 415, 165–174. https://doi.org/10.1016/j.epsl.2015.01.038.

Twitchett, R.J., 2001. Incompleteness of the Permian-Triassic fossil record: a consequence of productivity decline? Geol. J. 36 (3–4), 341–353. https://doi.org/10.1002/gj.883.

Twitchett, R.J., Looy, C.V., Morante, R., Visscher, H., Wignall, P.B., 2001. Rapid and synchronous collapse of marine and terrestrial ecosystems during the end-Permian biotic crisis. Geology 29 (4), 351–354. https://doi.org/10.1130/0091-7613(2001)029<0351:RASCOM>2.0.CO;2.

Utting, J., Spina, A., Jansonius, J., McGregor, D.C., Marshall, J.E.A., 2004. Reworked miospores in the upper paleozoic and lower Triassic of the northern circum-polar area and selected localities. Palynology 28 (1), 75–119. https://doi.org/10.1080/01916122.2004.9989592.

van Soelen, E.E., Kürschner, W.M., 2018. Late Permian to early Triassic changes in acritarch assemblages and morphology in the Boreal Arctic: New data from the Finnmark Platform. Palaeogeogr. Palaeoclimatol. Palaeoecol. 505, 120–127. https://doi.org/10.1016/j.palaeo.2018.05.034.

Villareal, T.A., Altabet, M.A., Culver-Rymsza, K., 1993. Nitrogen transport by vertically migrating diatom mats in the North Pacific Ocean. Nature 363 (6431), 709–712. https://doi.org/10.1038/363709a0.

Visser, P.M., Verspagen, J.M.H., Sandrini, G., Stal, L.J., Matthijs, H.C.P., Davis, T.W., Paerl, H.W., Huisman, J., 2016. How rising CO_2 and global warming may stimulate harmful cyanobacterial blooms. Harmful Algae 54, 145–159. https://doi.org/10.1016/j.hal.2015.12.006.

Volkman, J.K., 1986. A review of sterol markers for marine and terrigenous organic matter. Org. Geochem. 9 (2), 83–99. https://doi.org/10.1016/0146-6380(86)90089-6.

Volkman, J.K., 2003. Sterols in microorganisms. Appl. Microbiol. Biotechnol. 60 (5), 495–506. https://doi.org/10.1007/s00253-002-1172-8.

Volkman, J.K., 2005. Sterols and other triterpenoids: source specificity and evolution of biosynthetic pathways. Org. Geochem. 36 (2), 139–159. https://doi.org/10.1016/j.orggeochem.2004.06.013.

Volkman, J.K., Maxwell, J.R., 1986. Acyclic isoprenoids as biological markers. In: Johns, R.B. (Ed.), Biological Makers in the Sedimentary Record, pp. 1–42. Issue June.

Wang, Z., Fingas, M., 1995. Study of the effects of weathering on the chemical composition of a light crude oil using GC/MS GC/FID. J. Microcolumn Sep. 7 (6), 617–639. https://doi.org/10.1002/mcs.1220070609.

Wang, C., Liu, Y., Liu, H., Zhu, L., Shi, Q., 2005. Geochemical significance of the relative enrichment of pristane and the negative excursion of $\delta^{13}C_{Pr}$ across the Permian-Triassic Boundary at Meishan, China. Chin. Sci. Bull. 50 (19), 2213–2225. https://doi.org/10.1360/04wd0262.

Welander, P.V., Coleman, M.L., Sessions, A.L., Summons, R.E., Newman, D.K., 2010. Identification of a methylase required for 2-methylhopanoid production and implications for the interpretation of sedimentary hopanes. Proc. Natl. Acad. Sci. 107 (19), 8537–8542. https://doi.org/10.1073/pnas.0912949107.

Wignall, P.B., 2007. The End-Permian mass extinction – how bad did it get? Geobiology 5 (4), 303–309. https://doi.org/10.1111/j.1472-4669.2007.00130.x.

Wignall, P.B., Twitchett, R.J., 1996. Oceanic anoxia and the End Permian Mass Extinction. Science 272 (5265), 1155–1158. https://doi.org/10.1126/science.272.5265.1155.

Wignall, P.B., Twitchett, R.J., 2002. Extent, duration, and nature of the Permian-Triassic superanoxic event. In: Catastrophic Events and Mass Extinctions: Impacts and beyond, vol. 356, Issue October. Geological Society of America, pp. 395–413. https://doi.org/10.1130/0-8137-2356-6.395.

Wignall, P.B., Chu, D., Hilton, J.M., Corso, J.D., Wu, Y., Wang, Y., Atkinson, J., Tong, J., 2020a. Death in the shallows: the record of Permo-Triassic mass extinction in paralic settings, Southwest China. Glob. Planet. Chang. 189 (December 2019), 103176. https://doi.org/10.1016/j.gloplacha.2020.103176.

Wignall, P.B., Bond, D.P.G., Grasby, S.E., Pruss, S.B., Peakall, J., 2020b. Controls on the formation of microbially induced sedimentary structures and biotic recovery in the lower Triassic of Arctic Canada. Geol. Soc. Am. Bull. 132 (5–6), 918–930. https://doi.org/10.1130/B35229.1.

Wu, H., Zhang, S., Feng, Q., Jiang, G., Li, H., Yang, T., 2012. Milankovitch and sub-Milankovitch cycles of the early Triassic Daye Formation, South China and their geochronological and paleoclimatic implications. Gondwana Res. 22 (2), 748–759. https://doi.org/10.1016/j.gr.2011.12.003.

Wu, Y.S., Yu, G.L., Li, R.H., Song, L.R., Jiang, H.X., Riding, R., Liu, L.J., Liu, D.Y., Zhao, R., 2014. Cyanobacterial fossils from 252 Ma old microbialites and their environmental significance. Sci. Rep. 4, 1–5. https://doi.org/10.1038/srep03820.

Wu, Y.Y., Chu, D., Tong, J., Song, H.J., Dal Corso, J., Wignall, P.B., Song, H.Y., Du, Y., Cui, Y., 2021. Six-fold increase of atmospheric pCO_2 during the Permian–Triassic mass extinction. Nat. Commun. 12 (1), 2137. https://doi.org/10.1038/s41467-021-22298-7.

Xie, S., Pancost, R.D., Yin, H., Wang, H., Evershed, R.P., 2005. Two episodes of microbial change coupled with Permo/Triassic faunal mass extinction. Nature 434, 494–497. https://doi.org/10.1038/nature03396.

Xie, S., Pancost, R.D., Huang, X., Jiao, D., Lu, L., Huang, J., Yang, F., Evershed, R., 2007. Molecular and isotopic evidence for episodic environmental change across the Permo/Triassic boundary at Meishan in South China. Glob. Planet. Chang. 55 (1–3), 56–65. https://doi.org/10.1016/j.gloplacha.2006.06.016.

Xie, S., Pancost, R.D., Wang, Y., Yang, H., Wignall, P.B., Luo, G., Jia, C., Chen, L., 2010. Cyanobacterial blooms tied to volcanism during the 5 m.y. Permo-Triassic biotic crisis. Geology 38 (5), 447–450. https://doi.org/10.1130/G30769.1.

Xie, S., Algeo, T.J., Zhou, W., Ruan, X., Luo, G., Huang, J., Yan, J., 2017. Contrasting microbial community changes during mass extinctions at the Middle/late Permian and Permian/Triassic boundaries. Earth Planet. Sci. Lett. 460, 180–191. https://doi.org/10.1016/j.epsl.2016.12.015.

Yang, H., Chen, Z.Q., Wang, Y., Tong, J., Song, H., Chen, J., 2011. Composition and structure of microbialite ecosystems following the end-Permian mass extinction in South China. Palaeogeogr. Palaeoclimatol. Palaeoecol. 308 (1–2), 111–128. https://doi.org/10.1016/j.palaeo.2010.05.029.

Yin, H., Zhang, K., Tong, J., Yang, Z., Wu, S., 2001. The global stratotype section and point (GSSP) of the Permian-Triassic boundary. Episodes 24 (2), 102–114. https://doi.org/10.18814/epiiugs/2001/v24i2/004.

Zhang, Y., He, W., Feng, Q., 2007. A preliminary biogeochemistry-based quantification of primary productivity of end-Permian deep-water basin in Dongpan Section, Guangxi, South China. Front. Earth Sci. China 1 (4), 405–411. https://doi.org/10.1007/s11707-007-0049-7.

Zhang, S., Yuan, P., Zhao, L., Tong, J., Yang, H., Yu, J., Shi, Y., 2009. Clay rocks around Permian-Triassic boundary at Daxiakou section in Hubei Province, China. J. Earth Sci. 20 (6), 909–920. https://doi.org/10.1007/s12583-009-0077-1.

Zhang, Y.X., Wen, H., Zhu, C., Fan, H., Cloquet, C., 2018. Cadmium isotopic evidence for the evolution of marine primary productivity and the biological extinction event during the Permian-Triassic crisis from the Meishan section, South China. Chem. Geol. 481, 110–118. https://doi.org/10.1016/j.chemgeo.2018.02.005.

Zhang, G., Zhang, X., Shen, Y., 2021. Quantitative constraints on carbon cycling and temporal changes in episodic euxinia during the end-Permian mass extinction in South China. Chem. Geol. 562, 120036. https://doi.org/10.1016/J.CHEMGEO.2020.120036.

Zhao, L., Tong, J., Sun, Z., Orchard, M.J., 2008. Detailed lower Triassic conodont biostratigraphy and its implications for the GSSP candidate of the Induan-Olenekian boundary in Chaohu, Anhui Province. Prog. Nat. Sci. 18 (1), 79–90. https://doi.org/10.1016/j.pnsc.2007.07.001.

Zhao, L., Chen, Y., Chen, Z.Q., Cao, L., 2013. Uppermost Permian to lower Triassic conodont zonation from three gorges area, South China. Palaios 28 (8), 523–540. https://doi.org/10.2110/palo.2012.p12-107r.

Zhao, X., Tong, J., Yao, H., Niu, Z., Luo, M., Huang, Y., Song, H., 2015. Early Triassic trace fossils from the Three Gorges area of South China: Implications for the recovery of benthic ecosystems following the Permian–Triassic extinction. Palaeogeogr. Palaeoclimatol. Palaeoecol. 429, 100–116. https://doi.org/10.1016/j.palaeo.2015.04.008.

Zhao, T., Algeo, T.J., Feng, Q., Zi, J.W., Xu, G., 2019. Tracing the provenance of volcanic ash in Permian–Triassic boundary strata, South China: Constraints from inherited and syn-depositional magmatic zircons. Palaeogeogr. Palaeoclimatol. Palaeoecol. 516, 190–202. https://doi.org/10.1016/j.palaeo.2018.12.002.